AEROSPACE REPORT NO.
ATR-2017-01760

Investigation of the Nickel-Hydrogen Anomalous Heat Effect

May 15, 2017

Edward J. Beiting
Propulsion Science Department
Space Materials Laboratory

Prepared for:

Senior Vice President, Engineering and Technology Group

Authorized by: Engineering and Technology Group

PUBLIC RELEASE IS AUTHORIZED.

Acknowledgements

This work benefited from many interactions with Dr. Brian Ahern of Vibronic Energy Technologies. Dr. Martin Leung of The Aerospace Corporation arranged for the tomographic images of the filled cells and was a source of information for the chemical and isotopic analyses. Useful comments were provided by Drs. Brian Brady, John Desain, and Thomas Curtiss of The Aerospace Corporation and Drs. Richard Garwin and William Happer of the JASON group. Finally, Dr. James Nokes intervened to keep this work funded just as the data acquisition phase began. His support is gratefully acknowledged.

Executive Summary

Experimental work was undertaken to reproduce a specific observation of the gas-phase Anomalous Heat Effect (AHE)[*]. This task required the production of a quantity of heat energy by a mass of material so small that the origin of the energy cannot be attributable to a chemical process. The gas-phase form of AHE is difficult to reproduce and hence lacks a measure of credibility. The goal is to enhance its credibility by reproducing results first demonstrated in Japan and later reproduced in the U.S. by a solitary investigator. The technique heated nanometer-sized Ni:Pd particles (20:1 molar ratio) embedded in micron-sized particles of an inert refractory of ZrO_2. It was not within the purview of this work to investigate the physical origin of the AHE effect or speculate on its source.

An apparatus was built that comprised identical test and a reference heated cells. These thermally isolated cells each contained two thermocouples and a 10 cm^3 volume of ZrO_2NiPd particles. Calibration functions to infer thermal power from temperature were created by electrically heating the filled cells with known powers when they were either evacuated or pressurized with 1 bar of N_2. During the experimental trial, the test cell was pressurized with hydrogen and the control cell was pressurized with nitrogen. After conditioning the cells, both were heated to near 300°C for a period of 1000 hours (40 days). During this period, the test cell registered 7.5% more power (approximately 1 W) than the input power. The control cell measured approximately 0.05 W of excess power. The error in the excess power measurement was ±0.05 W.

Time-integrating the excess power to obtain an excess energy and normalizing to the 20 gram mass of the ZrO_2NiPd sample yields a specific energy of 173 MJ/kg. Assuming that the active material is the 5.44g of Ni+Pd yields a specific energy of 635 MJ/kg. For comparison, the highest specific energy of a hydrocarbon fuel (methane) is 55.5 MJ/kg. The highest chemical specific energy listed [see Energy Density in Wikipedia] is 142 MJ/kg for hydrogen compressed to 700 bar. Based on these results, it is unlikely that the source of heat energy was chemical in origin.

[*] The expression Anomalous Heat Effect (AHE) introduced by Dr. Robert Duncan will be used in this report to refer to a phenomenon often called Low Energy Nuclear Reactions (LENR), Condensed Matter Nuclear Science (CMNS), the old misnomer Cold Fusion, or several other names. The AHE moniker has the advantage that it only references the principal experimental manifestation while agnostic to the many theories attesting to its unknown physical origin.

Contents

Figures

Tables

1. Introduction

The study of the Anomalous Heat Effect (AHE) has a colorful history. Initially introduced via a press conference by two electrochemists in 1989 [1], it received worldwide attention due to the claim that the energy generated was orders of magnitude greater than that possible by chemical reactions. This energy was generated without producing radiation characteristic of nuclear reactions. Because the process occurred at low temperatures in an electrolysis cell, it was given the unfortunate moniker "Cold Fusion." This attracted numerous unsuccessful efforts to duplicate the results from the scientific community using an incomplete description of the experiment. Subsequently, the work was labeled junk science and the scientific hierarchy in the United States made it nearly impossible to publish or obtain funding for its study. However, studies did continue outside the U.S. and at low levels in the U.S. funded by non-traditional sources. Due to these subsequent studies, it is now understood why it was difficult to reproduce the energy releases observed the original electrolysis experiments. [2]

During these succeeding studies, a gas-phase manifestation of the AHE was discovered in Italy. [3] This is significant for two reasons. First, this new method used readily available nickel and light hydrogen instead of the expensive palladium and deuterium used in the electrolysis experiments. Second, the gas-phase experiments operated at much higher temperatures than the atmospheric-pressure heavy water electrolysis experiments, thus promising greater conversion efficiency to electrical or mechanical power. Unfortunately, most investigations of AHE have focused on electrolysis experiments leaving gas-phase AHE relatively unstudied. Consequently, critical parameters required for observing this manifestation are ill-defined. These include particle surface morphology, required hydrogen loading density, and triggering mechanisms. These known unknowns (and possibly other unknown unknowns) have made demonstrations of gas-phase AHE difficult to reproduce.

Because a practical implementation of the gas-phase AHE has the potential to transform the commercial and national security space industries by, for example, eliminating massive solar arrays, a small program was initiated at The Aerospace Corporation to see if the AHE could be observed in our laboratory. Because it was an internally funded modest program, the goal was not to create a research effort to study its origin but to demonstrate reproducibility of previous work. If demonstration was successful and convincing, the hope was that this work would stimulate a subsequent larger effort.

To this end, a review of the gas-phase AHE results was made when this project was initiated in 2013 to find an observation likely to be reproduced. Three criteria were considered to increase probability of achieving this goal: a complete description of material preparation was required; a simple triggering mechanism was desirable to reduce the experimental complexity; and at least one reproduction of the manifestation of excess heat[†] of non-chemical origin using the method should be documented by an independent investigator. At the time of this survey, only the work by Arata and Zhang [4] in Japan as reproduced by Ahern [5] in the United States met these three requirements.[‡] This method employs a simple heat-triggering mechanism on a powder of micron-sized particles of ZrO_2 imbedded with nanometer-sized particles of a nickel (with a small admixture of palladium). The active material used in the work presented in this report differs from that of Refs. [4] and [5] by the addition of magnetic particles. This addition was made with the desire of increasing the probability of observing excess energy, based on reports by other investigators

[†] Most AHE experiments require input heat power to raise the temperature of the sample material to a value above a critical temperature. If more heat is generated than supplied to the sample, this difference (exothermic) heat is called "excess heat." If the integrated excess heat power over the duration of the experiment (= excess energy) is more than can be attributed to chemical energy, the observation of the AHE is considered positive.

[‡] We note since this work was initiated, other demonstrations of the AHE of NiPd nanoparticles in a ZrO_2 matrix have been documented. Examples can be found in Special Section: Low Energy Nuclear Reactions of Current Science Vol. 108 No. 4 (2015) available at:
http://www.currentscience.ac.in/php/feat.php?feature=Special%20Section:%20Low%20Energy%20Nuclear%20Reactions&featid=10094

[6] and the initial experimental trial in this work. Other than these additional particles, the material used here was identical to that used by Refs. [4] and [5].

The tasks undertaken to implement this demonstration include base material acquisition and sample fabrication, design and construction of the computer-controlled experimental apparatus, creation of robust data acquisition (DAQ) software, system calibration, extended periods of data acquisition, and data analysis and interpretation. Completion of these tasks produced two experimental trials, each using two parallel cells controlled and monitored by a single DAQ computer. The first trial served primarily as a learning vehicle for developing and testing an experimental protocol. Its results are not discussed in the body of this report; however, its design, with lessons learned, and the data produced during this 23-day run are interesting so its description is presented in Appendix A.

The duration of second experiment trial was over 1600 hours (67 days). It is described in detail in the report preceded by sections presenting the preparation of the sample and the description of the apparatus. The final section of the report presents an error discussion and conclusions. To improve the readability of the body of this document, many details are presented in nine appendices.

2. Sample Preparation

The samples were prepared following a prescription described by Ahern [5], who drew his procedures from those developed by Arata and Zhang [4]. This type of preparation was developed for the fabrication of catalysts, which require large metallic surface areas that operate at high temperatures. Large specific areas require small particles that will sinter into large particles at high temperatures. Thus techniques were developed to imbed small metallic particles in large porous inert refractory particles.

Figure 2.1. Approximately 10 grams of 65wt% Zr- 32wt% Ni-3wt% Pd alloy melt spun ribbon in a 1L breaker used for furnace oxidation.

The base metallic material was prepared by Ames Laboratory [7] by arc melting a 90 gram mixture of 65wt% Zr 32wt% Ni 3wt% Pd using 99.95% purity elements. This hot composite was melt-spun onto a water-cooled copper hearth plate in an atmosphere of high purity argon using a wheel speed of 25 m/s and an ejection pressure of 110 Torr. This procedure was repeated, each run creating approximately 10 grams melt spun ribbons. A view of ribbon from one of these spins is shown in Figure 2.1.

At The Aerospace Corporation ribbon from a 10 gram single run was placed in a furnace and heated in air at 440°C for 28 hours. This created approximately 12 grams of brittle material comprising nickel and palladium nano-particles in a ZrO_2 matrix. This material was hand-ground in a mortar and pestle for a few minutes creating jagged particle with diameters of a few hundred microns in diameter. Subsequently the ground sample was placed in a 45 mL zirconia ceramic vial with two 12.7 mm diameter zirconia balls and ground in mixer/mill [8] for 4 minutes. Macroscopic and microscopic views of the sample before and after it was placed in the mill are shown in Figures 2.2 and 2.3, respectively. The mill created particles that were a few microns in diameter with a few as large as 40 microns. Milling the sample for less than 4 minutes left many large jagged particles. Milling for 4 minutes ground most of the large particle but generally created particles smaller than the targeted 10–30 micron diameter size distribution.

Figure 2.2. ZrO_2NiPd after ground with a mortar & pestle (center) and 4 minutes in power grinder (right). The left sample is the SmCo magnetic after it was ground with a mortar & pestle

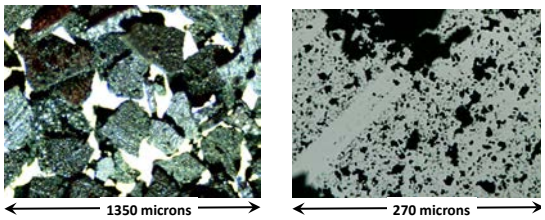

ZrO_2NiPd Mortar & Pestle ZrO_2NiPd 4 min in Grinder

Figure 2.3. Microscopic images of ZrO_2NiPd samples shown in Figure 2.2.

There have been reports that a magnetic field can enhance the AHE (for example, see Ref. [6]). To explore this possibility, for the first experiment it was decided to run a second cell loaded with magnetic material in parallel with the first. The material in this cell was a mixture of approximately equal weights of a milled SmCo 2-17 magnet and the ZrO_2NiPd sample described above. A discussion on the choice of a SmCo magnet rather than a NdFeB magnet which usually has a higher magnetic field strength is given in Appendix B.

Because the magnet particles stick together tightly in a single mass after they are ground, the ZrO_2NiPd sample and the magnetic sample were placed together in the Mixer/Mill after they were individually ground in the mortar and pestle. The hope was that milling them together would facilitate their mixing. This was partially successful. A view of the mixture of the SmCo magnet particles with the ZrO_2NiPd sample is shown in Figure 2.4. In this photo the large particles are the SmCo, and ZrO_2NiPd particles are on the surface of the magnet particles.

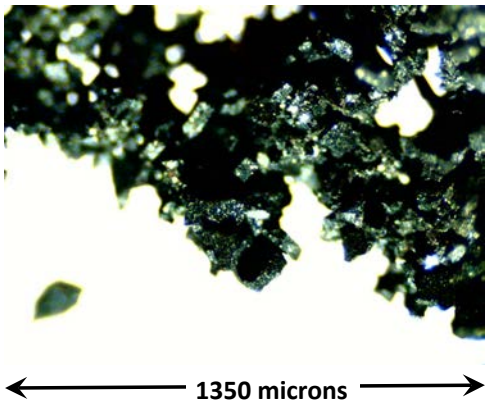

Figure 2.4. Microscopic image of ZrO_2NiPd+ SmCo after 4 min in mixer/grinder

3. Experimental Design

The method chosen for gas-phase AHE reproduction required only thermal triggering. This required building cells that could be heated in vacuum to temperatures near 400° C. The design described here accomplishes this principally using off-the-shelf parts.

The cell design used in the first experimental trial (described in Appendix A) is shown in Figure 3.1. It uses a Swagelok 10 cc stainless steel sample cylinder, standard Swagelok fittings, mounted on a 2.75 inch diameter conflat flange. This flange is installed on a standard 5 inch long x 1.5 inch diameter stainless steel (SS) nipple with a 2.75 inch conflat flanges on both ends. The guiding principle was to build a thermally isolated container for the sample that has little heat capacity so that a small energy release will cause a large, easily measured temperature rise. The volume around the sample cylinder is evacuated by a mechanical pump[§] whereas the interior of the sample cell is evaluated to a few microbar (mTorr) using a turbo-pump backed by a diaphragm pump, keeping the sample oil free. The 3/8 inch Swaglock fitting connecting the sample cylinder to the conflat flange was a poor thermal insulator, producing some conduction heating the outer vacuum cylinder.

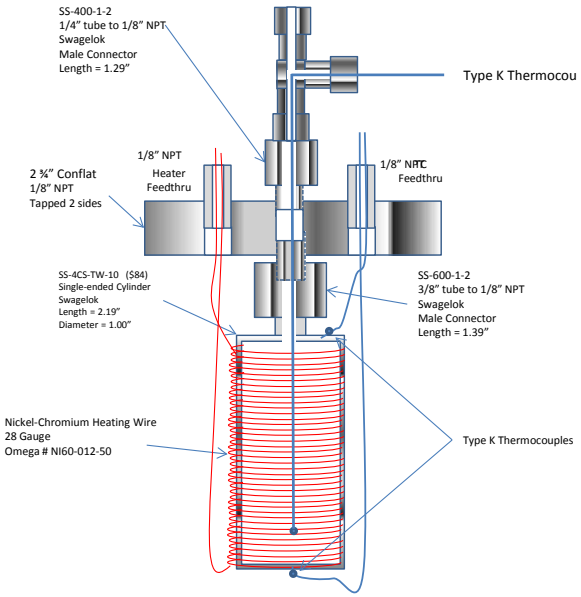

Figure 3.1 Diagram of the test cell design.

The small size of the configuration required that feedthroughs for the power leads and thermocouples be custom made. Unfortunately, suitable thermocouples could not be purchased so they were made in-house by torch fusing 0.010" diameter chromel-alumel wire (type K) and using a combination of porcelain beads and glass-sleeve high-temperature insulators. One of the interior cell feedthroughs and thermocouple is shown in Figure 3.2 mounted on ¼ inch Swagelok fittings.

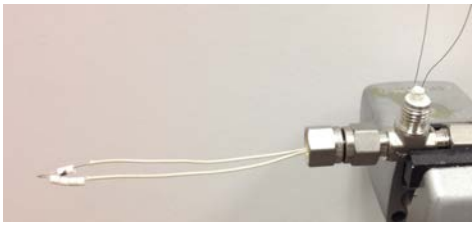

Figure 3.2 Custom feedthrough and thermocouple used for interior cell temperature measurements.

As shown in Figure 3.1, the sample cylinder was spiral wound with bare nichrome wire. It was desired to electrically insulate this wire from the SS cylinder while keeping good thermal conductivity to the cylinder. Initially, the cylinder was coated with high-temperature paint before wrapping the wire. (See Figure 3.3.) Of several coatings tried, Aremco [9] Pyro-Paint 634-ZO worked the best.

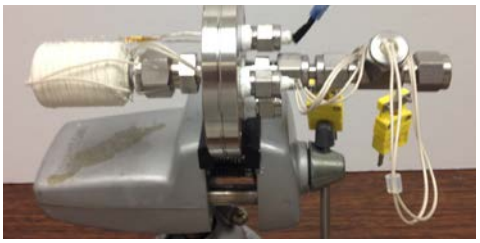

Figure 3.3 Photograph of version on of cell mount on 2.75 inch conflat flange.

[§] The mechanical pump available had a rather high base pressure of 0.08 mbar (60 mTorr). This reduced the thermal conductivity of the air by only 30%, whereas a well-maintained two-stage rotary vane pump would have reduced by thermal conductivity of air factor of 24 from the atmospheric pressure value. See Appendix I.

However, even though this paint is rated for a temperature of 1800°C, it repeatedly failed causing the circuit to short when the interior cell temperatures reached 400°C. Subsequently, the nichrome wire was threaded through a woven glass sleeve [10] and then wrapped round the cylinder as shown in Figure 3.4. This configuration proved robust, allowing calibration to be performed up to 450°C. The nichrome wire (OMEGA PN NI60-012-50, NI60.CR16) [11] had a room temperature resistance of 4.359 Ω /ft. Cell #1 in the experiments described below had a resistance of 14.9 Ω and cell #2 a resistance of 15.3 Ω. Accordingly, when the power suppliers were used in constant voltage mode, the power delivered to the cells differed slightly.

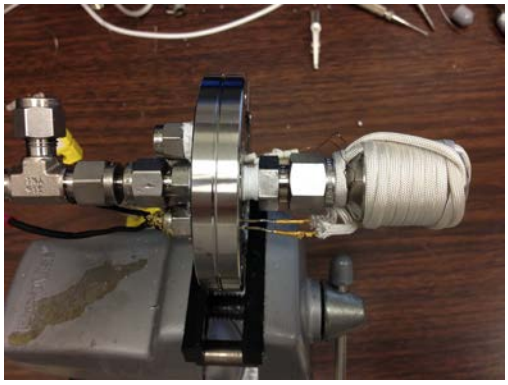

Figure 3.4 Glass sleeve insulated heating wire.

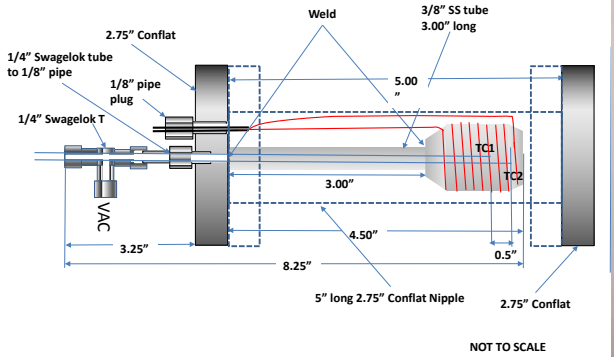

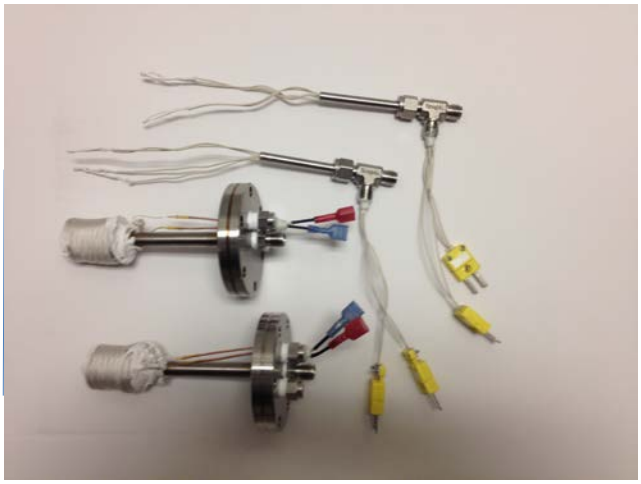

Figure 3.5 Design and photographs of the welded cell configuration and the thermocouple inserts.

Applying the lessons learned from the first experimental trail as discussed in Appendix A, the cell design was modified. Figure 3.5 shows the design (left) and a photo (right) of the cells and thermocouple inserts used in the principal (second) experimental trial. Again the cell assemblies were designed to fit inside a standard 2.75 inch conflate nipple SS vacuum jacket. The wall the SS cells were thinned to about half of their original thicknesses to reduce the heat capacities, temperature gradients, and decrease the thermal time constants. The thermocouples were coated with high temperature Aremco Pyro-Paint 670 and threaded through the SS tubing. Using longer tubes to support the cells and inserting two thermocouples instead of one in a cell made filling the cells with the 26 grams of the material tedious. Unfortunately, initial vacuum tests on the new cells indicated a vacuum leak in one of them. Because time did not permit new part acquisition and building another cell, this leak was patched with Torrseal.

The cells were loaded with the samples, the interior thermocouples installed into the cells, and the cells were placed in their individual vacuum jackets. Subsequently, the assemblies were installed in the gas manifold shown in Figure 3.6. The interior of the cells were evacuated with a Varian minitask pump comprising a 70 L/s turbo pump backed by a diaphragm pump creating an ultimate pressure just above the pump orifice of a few tenths of a microbar[**] (millitorr). As noted, this system created an oil-free vacuum.

[**] The principal unit for pressure used in this document is "bar." For conversion to SI units 1 bar = 100 kPa exactly and is referenced to vacuum.

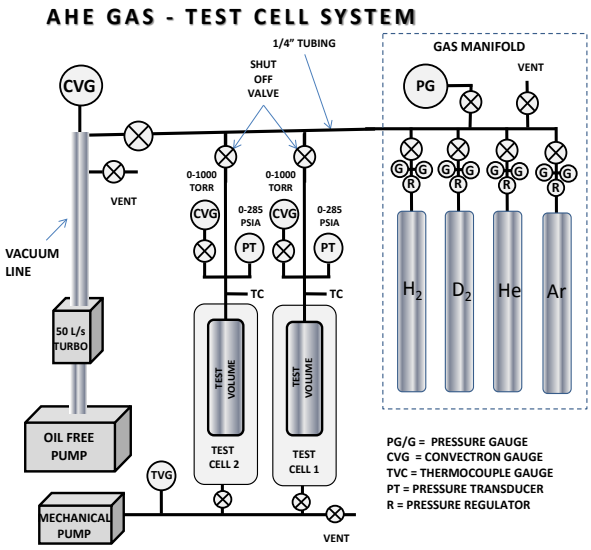

Figure 3.6 Gas system.

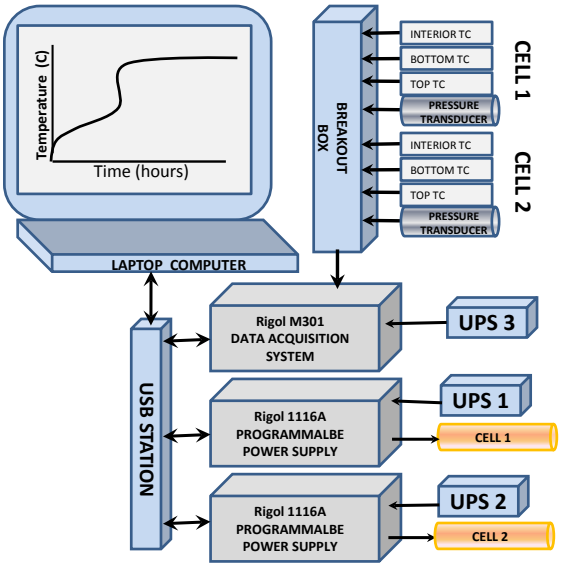

Figure 3.7 Data acquisition system.

Figure 3.7 shows the power and data acquisition systems. The power is delivered individually to each cell by two Rigol 1116A computer controlled power supplies operated in constant voltage mode. The voltage, current, and power delivered is that reported by the instrument; the voltage and current values were checked with an Agilent 34301A multimeter (IBS ABE983, Cal Due Date 2/21/16) and agreed to ± 0.002 V, ± 0.002 A).

The Rigol M301 data acquisition system read the voltages from the pressure transducers and the thermocouples. The two pressure transducers [12] had a voltage output range of 0 – 5 V to cover the pressure range of 0 to 285 PSIA (20 bar). The Rigol M301 temperature output values of the type K thermocouples were calibrated (adjusted) at 0°C (ice bath) and 240° C (hot glycerin) with a linear function using an Omega HH309A thermocouple readout (IBS ACH235, Cal Due Date 6/14/15).

Although the Rigol M301 DAQ system is well documented to supply a reference junction for the temperature measurements, it did not. Consequently, there could be variations with the reported temperature if the room temperature were to change. The room temperature was monitored throughout the data acquisition period and compensation was made during the data analysis. This is discussed further in the next section. It is estimated that the temperatures are accurate to ± 0.5°C.

All communication to the Rigol instruments was through a USB port on a laptop computer. The instrument controlling software was written in MATLAB® using the MATLAB Instrument Control Toolbox, which sent SCPI text commands that were recognized by the instruments. Intermediate results of a few hours could be viewed as a series of strip-chart graphs on the computer screen. The results from the entire experimental run could also be viewed on another set of graphs on the screen albeit with lower temporal fidelity. Data were taken at 30 second intervals and appended to a data file, ensuring that any experimental interruption would not result in a loss of data. This file could be downloaded for detailed analysis at any time without interrupting the experiment.

Due to the long duration of a continuous data acquisition period, an important element in the experimental configuration was the uninterruptible power supplies (UPS). The battery in the laptop computer made the this controller immune to power interruptions but each of the Rigol instruments required an individual UPS to allow the experiment to operate through a loss of grid power of at least two hours. There were two power interruptions during the experimental runs. Any interruption would have compromised the results.

4. Principal Experiment Trial

To increase credibility of the second trial results, the active test cell and an inert reference cell were loaded with identical material. However, the test cell was pressurized with hydrogen and the reference cell with nitrogen. The mass of the ZrO_2NiPd powder in each cell was doubled from the first trial to 20 grams. Furthermore, since the first experimental trial indicated that the magnetic particles may have increased the generation of the excess heat (see Appendix A), a sufficient mass of SmCo particles (6 grams) was added to fill the remainder of the 10 cm^3 cell volume. Other differences from the first trial were the use of hydrogen instead of deuterium gas and ZrO_2NiPd powder as ground to < 1 μm diameter.

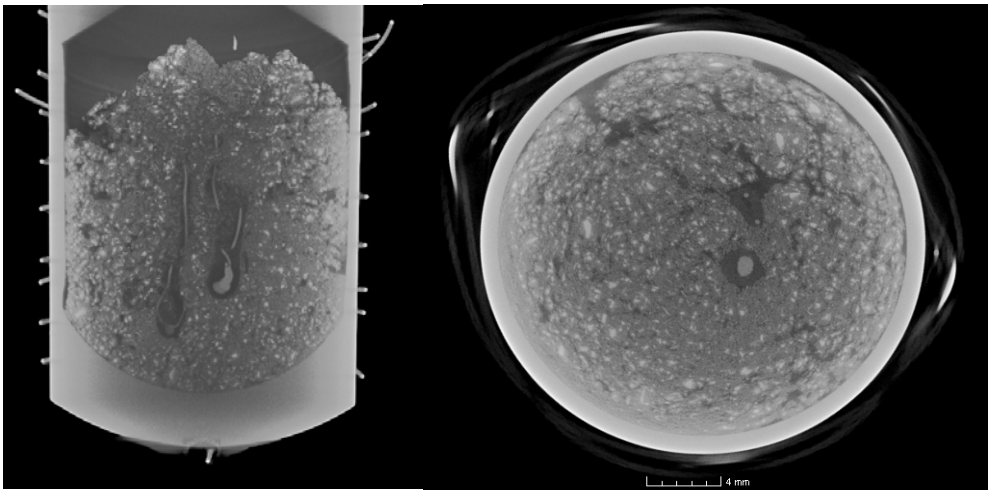

Figure 4.1 Cell 1 vertical and horizontal slices from the x-ray tomographic images.

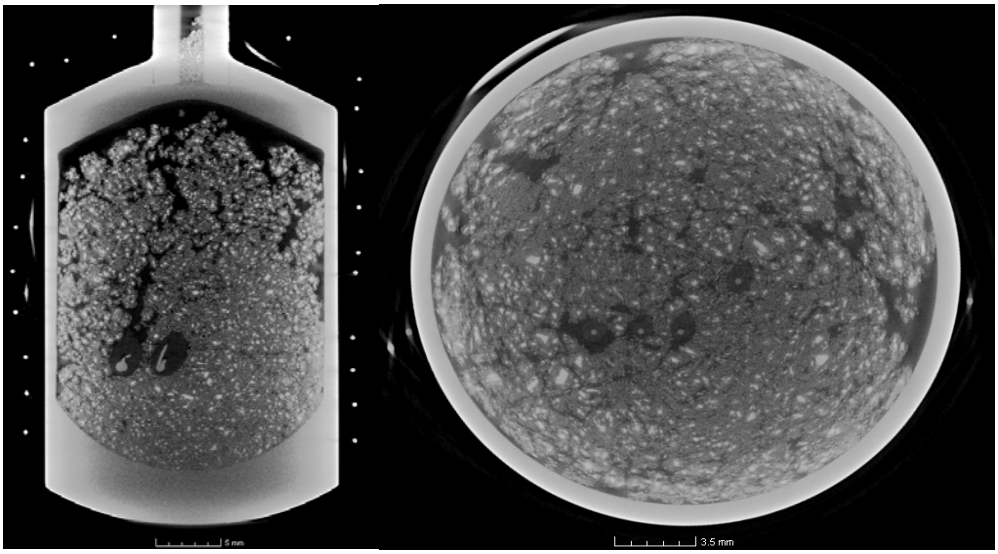

Figure 4.2 Cell 2 vertical and horizontal slices from the x-ray tomographic images.

Figures 4.1 and 4.2 show slices form the 3D x-ray tomographic imaging taken of cell #1 and cell #2, respectively. Images of both cells show that some of the material remained in the neck of the cells. This trapped material was later pushed into the cell using a fine wire, filling the remainder of the cells without disturbing the material and thermocouple placement in the body of the cells. These images show the thermocouples are separated by at least 3 mm from each other and each are displaced from the cell walls. The high atomic weight SmCo magnetic particles appear as bright particles in these images

4.1 Bakeout and Calibration

After installation into the experiment apparatus (Figure 3.6), the cells were evacuated for bake-out. The vacuum bake-out comprised a period of 20 hours between 160°C and 260°C and 22 hours between 320°C and 340°C. The highest pressure registered during this procedure was 22 mTorr (0.03 mbar) at 300°C, after which the pressure decreased to 4 mTorr (0.005 mbar) even as the temperature increased to 340°C. After cooling to room temperature the pressure of the cells was near 1 mTorr (0.0013 mbar).

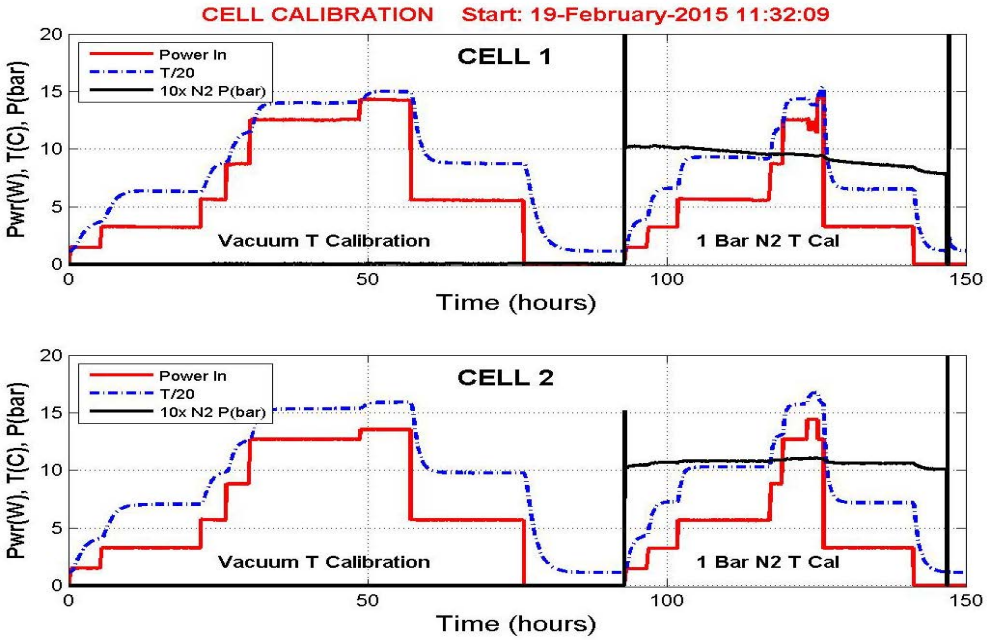

Figure 4.3 Power, temperature and pressure during calibration.

After bakeout, the recorded trial run of duration 1610 hours (67 days) began. The data from this period are discussed sequentially. Calibration began at time zero. The power, temperature and pressure curves of the cells during calibration are shown in Figure 4.3. Note that it requires several hours to reach an equilibrium temperature after a power change. For the temperatures where full equilibrium was not reached, a small extrapolation was used to obtain the equilibrium temperature. Better thermal isolation of the cell increases the time to reach equilibrium. Note the nitrogen pressure curves during the 1 bar calibration. In cell 2, the pressure remains constant except for small variations with temperature. If the entire volume of the gas were heated from room temperature to 300°C, one would expect a 2X increase in pressure. The

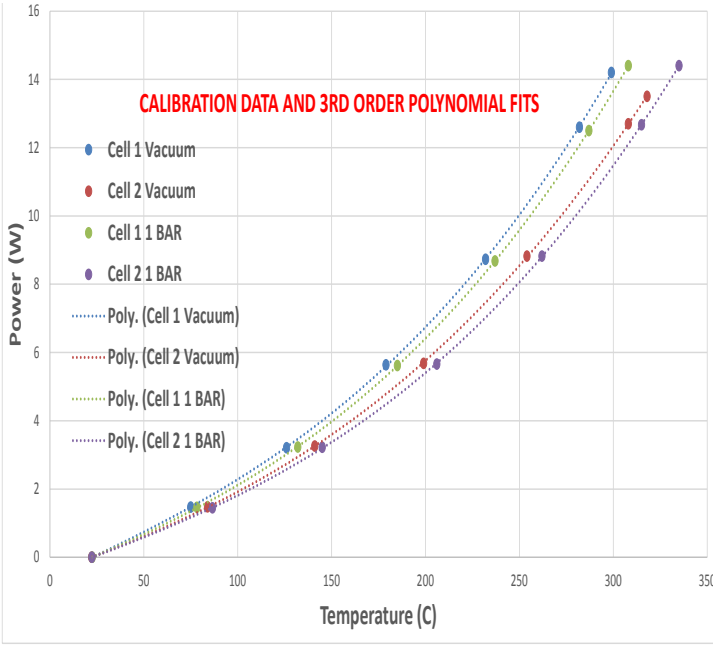

Figure 4.4 Calibration curves used to infer power from cells 1 and 2 for in vacuum and at a pressure of 1 bar of nitrogen.

increase of 0.1 bar at 340°C indicates that only about 10% of the gas volume is heated; the remainder is in the unheated gas manifold. There is a slight indication of a lower pressure after the cell 2 returns to room temperature, which indicates a pressure decrease rate of about 0.5 mbar/hr. In cell 1 the N_2 pressure decreases at a rate of about 0.2 bar/50 hours = 4 mbar/hr. This could indicate a leak with a rate of 0.4%/hr if independent of pressure.

Eight calibration curves were created, one for each thermocouple in each cell in vacuum and at 1 bar N_2 gas. However, because there was no significant difference between the calibration curves for the two thermocouples in a given cell there are effectively only four curves.

These four calibration curves for the cells are given in Figure 4.4. Note that the difference between the calibration curves for the two cells is significant as is, to a lesser degree, the difference for a given cell for the two pressures. At temperatures between 250°C and 300°C, the range of temperatures where the experiment was operated, the system sensitivity is between 12°C/W and 13°C/W, about 50% better than that of the first experiment. The third order polynomials used to generate the curves shown in Figure 4.4 and used to infer the power from the temperature are:

$$\begin{aligned} \mathrm{PwrC_1T_1Vac} &= 0.0000002467\ T^3 + 0.0000055991\ T^2 + 0.0256426972\ T - 0.5841432429 \\ \mathrm{PwrC_2T_1Vac} &= 0.0000001592\ T^3 + 0.0000266273\ T^2 + 0.0193175282\ T - 0.4392951681 \end{aligned} \quad (1)$$

$$\begin{aligned} \mathrm{PwrC_1T_1N_2} &= 0.0000002121\ T^3 + 0.0000200707\ T^2 + 0.0220929047\ T - 0.5067000132 \\ \mathrm{PwrC_2T_1N_2} &= 0.0000001930\ T^3 + 0.0000082186\ T^2 + 0.0199322732\ T - 0.4540048955 \end{aligned}$$

The fits for these polynomials had R^2 values of greater than 0.99999.

Table 4.1: Vacuum vs Pressure Calibration Comparison for Cell 1

T (ºC)	Vac Pwr (W)	1 bar N_2 Pwr (W)	Diff (W)
50	0.613049	0.58728	0.025769
100	1.917931	1.814408	0.103522
150	3.594748	3.37213	0.222619
200	5.762902	5.405194	0.357709
250	8.541793	8.058351	0.483442
300	12.05082	11.47635	0.574469

It is interesting to compare the difference between the vacuum and 1 bar N_2 calibrations for a given cell. This is done in Table 1 for cell 1. This difference in inferred power goes from an insignificant 0.03 W at 50°C to a significant 0.6 W at 300°C, with the inferred power for the vacuum case greater than that of the 1 bar N_2 case. That is, it requires more power to achieve a given temperature if the cell is at a lower pressure than a higher pressure after the cell has reached thermal equilibrium. A possible explanation is that the nitrogen creates a more efficient thermal path between the heater wires and the thermocouples and this effect is greater than the increase in the conductive loss path cooling the thermocouple. This would imply a thermal gradient exists in the cell after equilibrium is reached. Another possible explanation is that nitrogen gas is reacting exothermically with one or more of the compounds; i.e., ZrO_2, Ni, Pd, SmCo or possibly Zr that was not converted to ZrO_2 (N_2 does react with Zr to create ZrN; for example,

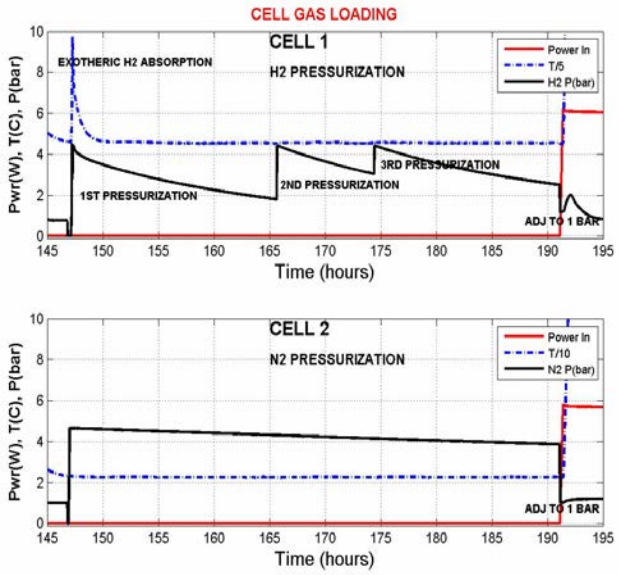

Figure 4.5 Gas loading curves.

see Ref. [13]). However, this second scenario is considered unlikely. The origin of this difference will remain speculative but the assumption will be made that whatever its origin it does not change during the course of the experiment and the calibration curves can be used to infer the power.

4.2 Conditioning and Hydrogen Loading

The cells were then loaded with gas, H_2 in cell 1 and N_2 in cell 2 as shown in Figure 4.5. The loading pressure was nominally 4.5 bars. The heat capacity for both gases is nearly the same but the thermal conductivity of hydrogen is 7 times greater than that of nitrogen at room temperature (see Appendix C and the end of Section 5). In cell 2, we observe a constant decrease in N_2 pressure at a rate of 15 mbar/hr with the cell remaining at a constant temperature. This is much larger than the pressure decrease rate of 0.5 mbar/hr seen in cell 2 during the N_2 calibration run. In cell 1, the H_2 loading was done in three steps resulting in pressure decrease rates of 137 mbar/hr, 187 mbar/hr, and 105 mbar/hr. These rates are also much larger than the 4 mbar/hr rate observed for this cell during the N_2 calibration run. Finally we note the 25°C temperature rise in cell 1 at the beginning of the first H_2 loading. Loading H_2 into nickel or palladium is an exothermic process and this temperature rise was routinely observed in loading into this ZrO_2Ni powder. [5]

The data in Figure 4.5 can be used to estimate the hydrogen gas absorbed. Noting that the change in pressure due to the three pressurizations = 2.6 +1.5 +1.9 = 6.0 bar, and assuming only 20% of the volume 10 cm^3 cell is empty and the gas manifold has an estimated volume of 8 cm^3, the total volume is approximately 10 cm^3. Then from the ideal gas law, the number of moles of H_2 absorbed is

$$n_{H2} = 6 \text{ bar} \times 10 \text{ cm}^3/(2.24 \times 10^4 \text{ cm}^3\text{-atm /mole} \times 0.987 \text{ bar/atm}) = 2.7 \times 10^{-3} \text{ mole of } H_2$$

The moles of n_{Ni} = 4.98g/58.7 g/mole = 0.11 moles (see Appendix F). Assuming that only the nickel atoms adsorb the atoms of hydrogen then the fraction of Ni atoms with H atoms is moles of H atoms/moles of Ni = 2 x 2.7 x 10^{-3} mole of H_2/0.11 = 4.9%. This represents an upper limit on the number of Ni atoms with H atoms as there could be H_2 loss to other mechanisms. As noted below, it is likely that most of the hydrogen is adsorbed by the palladium. There are 4.32 x 10^{-3} moles of Pd in the cell (Appendix F); if all the hydrogen atoms were adsorbed by palladium, the palladium loading would be about 125%, indicating that some of the hydrogen atoms are adsorbed in the Ni or elsewhere.

It is instructive to calculate the amount of energy added to the cell due to work of $\Delta P \times V$. Using 6 bars for the pressure change and 10 cm^3 for the volume we obtain 6 J. During the 40-hour loading period, the average power is 4 x 10^{-5} W. Near room temperature the cell constant is 27°C/0.7 W = 38°C/W. The resultant temperature change of 0.002°C would not be observable.

The exothermic energy causing the temperature rise seen in the upper graph of Figure 4.5 near 147 hours is calculated to be 1120 J (see Appendix G). Assuming that 100kJ/mole of energy is released when adsorbed by the surface of Pd [14] implies 0.011 moles of H_2 are adsorbed by Pd. This is four times the value of hydrogen calculated in the adsorption estimate above.

4.3 Power Ramp-up Period

After the calibration and fill, the power run was initiated to trigger the AHE. This is done using two computer-controlled regulated DC power supplies (Rigol Model 1116A) in voltage regulated mode to heat the nichrome wire heaters wound around the sample cells. The voltage was set to different values for the two cells in order to have approximately the same registered temperature in each cell. The input power to each cell was recorded from power supply digital output, which was found to be accurate to better than 0.1% by comparing to an Agilent calibrated multimeter.

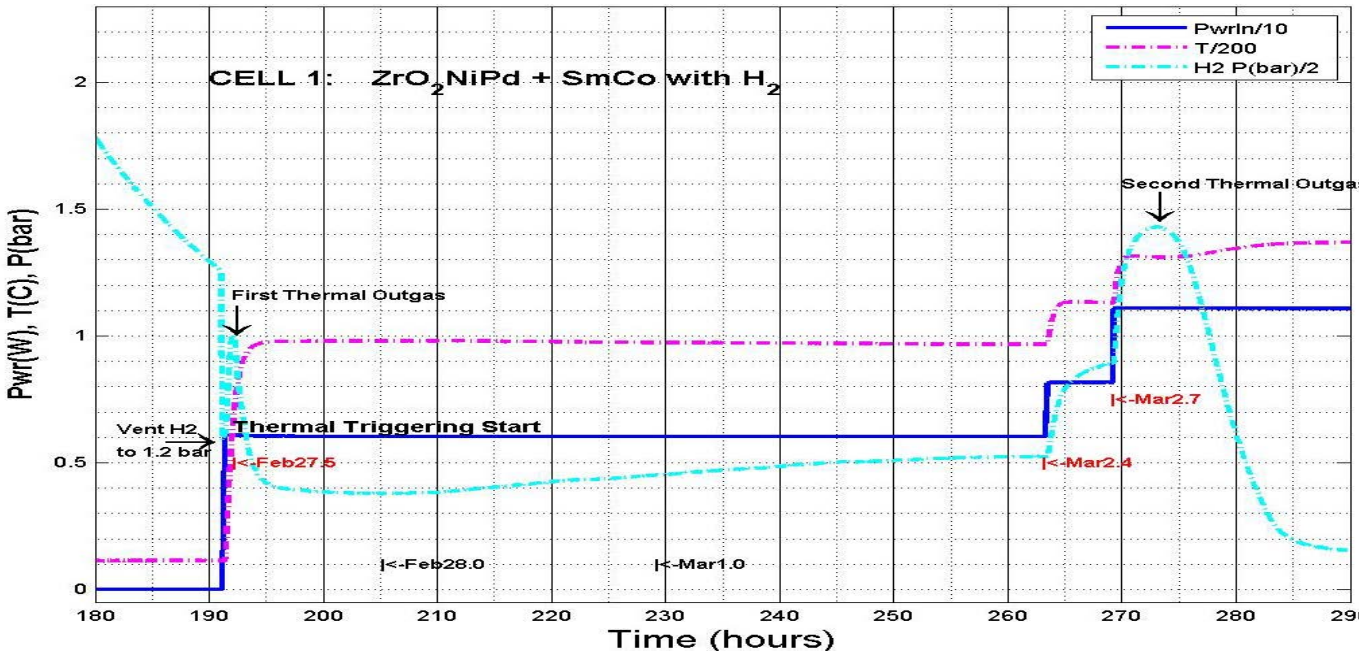

Figure 4.6 Hydrogen cell during preheating.

It is worth studying the power ramp up period that took place between 190 and 270 hours for the hydrogen cell (#1). These data are shown in Figure 4.6. Date/times are marked on this graph; the times appearing red indicate the times where the power or pressure was changed. The left of the graph shows the end of the loading period given in Figure 4.5. Near 191 hours the hydrogen pressure was vented to pressure of 1.2 bar and 6 W of power was applied to the cell heating coil raising its internal temperature to just under 200°C. This temperature rise caused the (presumably H_2) pressure to rise to 2.0 bars; subsequently this hydrogen was reabsorbed over the next 5 hours reaching a minimum pressure of about 0.8 bar. Over the next 65 hours as the cell continued to be heated, this pressure gradually increased to a value slightly above 1 bar at 263 hours when the heater power was again increased in two steps resulting in a two-step increase in the pressure, peaking at a value of greater than 2.8 bars at 273 hours. This pressure decreased rapidly for the next 10 hours reaching to 0.6 bar at 290 and continued to decrease slowly to a value of < 0.05 bar at 1650 hours as seen below.

One may speculate to the cause of these pressure variations. As noted in Section 2, the active material in the cells is nano-particles of nickel and palladium metal in a matrix of ZrO_2 micron-sized particles, the mole ratio of Ni:Pd being 19.6:1. However, hydrogen solubility is 10^5 times greater in Pd than in Ni at 200°C and greater at lower temperatures. [15] Thus it is likely that most of the hydrogen was absorbed by the palladium during the room temperature loading period and, when heated, a significant amount of this hydrogen was released. This is, of course, the mechanism used for hydrogen storage and retrieval in palladium. [16] During the course of the reabsorption, some of this hydrogen was absorbed by the nickel. Absorption of hydrogen in Ni is largely a surface effect whereas it is a volume effect in Pd.

4.4 Power Generation Period

Figure 4.7 shows the data for both cells during the portion of the run dedicated to measuring the excess heat power and energy. This interval lasted approximately 1000 hours (42 days). The scaling for each of the data traces is given in the legend. The temperature of each cell is shown by the magenta trace and the input power is depicted by the blue line. The light blue line records the pressure in units of bar. The red trace records the excess power; that is, the power inferred from the cell temperature using the appropriate calibration algorithm minus the input power.

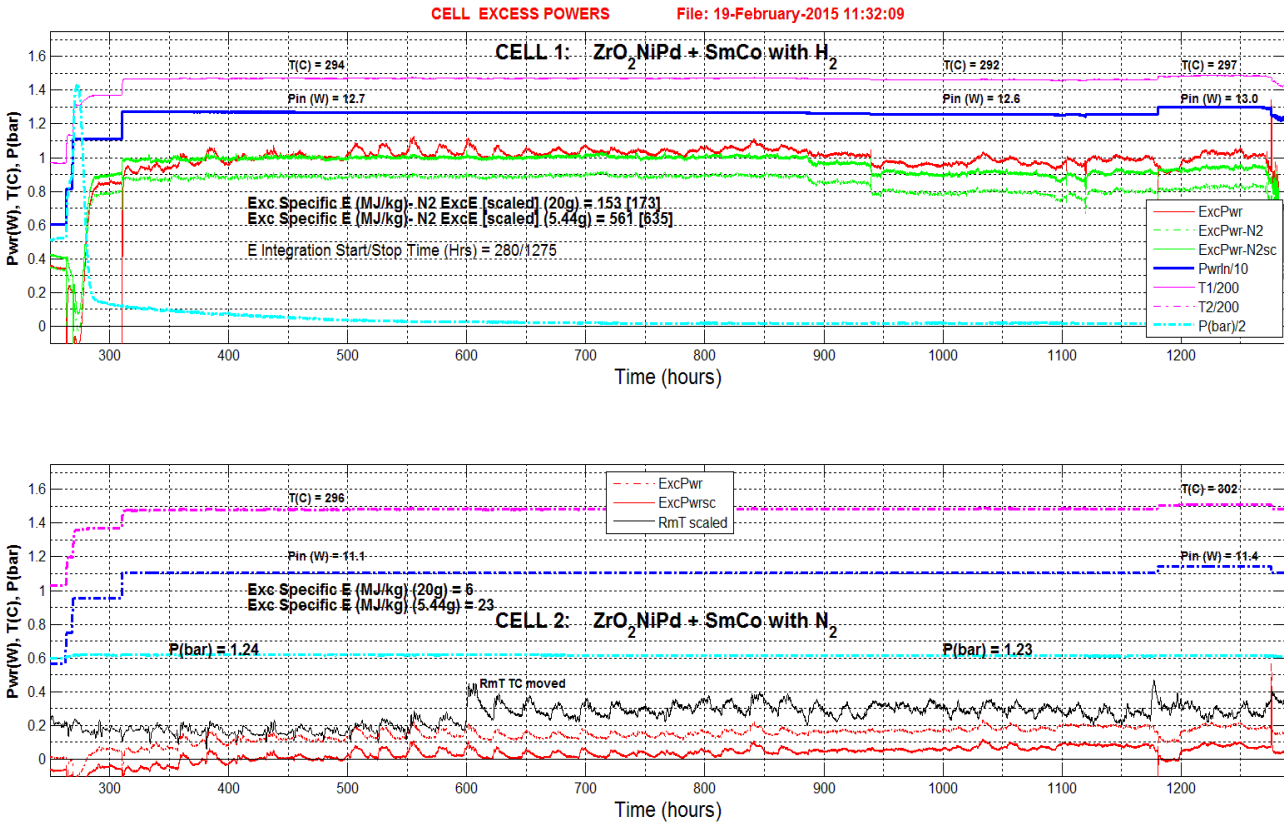

Figure 4.7 Power, temperature, and pressure data from hydrogen (cell 1) and nitrogen (cell 2) cells.

We begin with a few general observations. First we see that the light blue pressure traces indicate the pressure in the hydrogen cell asymptotically approaches zero where the pressure in the nitrogen cell remains nearly constant during the 1050 hour interval shown. Also note that cell 1 required 1.6 watts additional power to maintain the same temperature as cell 2. This is consistent with the calibration data shown in Figure 4.4 for the cell 1 vacuum calibration and the cell 2 1-bar calibration. The difference between the interior thermocouple temperatures (T1-T2) during the energy integrations period was -0.3 ±0.1°C and -0.5 ±0.1°C for cells 1 and 2 respectively (see Appendix D).

The red traces depict the excess power calculated by using the thermocouple reading from the cell interior to infer the cell heat power (employing the vacuum calibration algorithm for cell 1 and the 1-bar algorithm for cell 2) and subtracting the input power recorded for the respective cells (i.e., $P_{excess} = P_{inferred} - P_{in}$). These traces show large excursions from their mean values whenever the power (i.e., temperature) was changed. This is because the algorithm used equilibrium temperatures and 3+ hours are required to reach this equilibrium. During this transition period, a large negative excursion appeared for an increase in applied power and a positive excursion for a decrease in applied power.

Note that both red excess power traces show a 24 hour periodicity. The light black trace on the cell 2 (lower) plot is an arbitrarily scaled ($\Delta = 0.2$ in ordinate = 1°C) thermocouple reading that recorded the room temperature near the cells (the apparent shift of 0.5°C at 600 hours is due to changing the location of this thermocouple). The peak-to-trough magnitude of this room temperature curve is on the order of 1°C. The variation in the red excess power traces are between 0.05 and 0.1 W indicating a temperature variation of about 1°C. As noted in Section 3, the temperature algorithm of the Rigol DAC instrument that converted the mV thermocouple output to temperature did not use a correct reference junction definition. It is speculated that the periodicity observed in the excess power curves is due to the changing room temperature that resulted in error in the inferred temperature and hence inferred power. In any case, the variation in the

excess power is at most 100 mW or 10% of the excess power. This variation is removed by the subtraction of N_2 cell excess power, reducing the H_2 cell excess power as discussed below.

A more troubling observation is the 100 to 200 mW of inferred excess power from the nitrogen cell shown in the lower graph. This cell is the control experiment where no excess heat is expected. If we assume that excess heat is the systematic error in the experiment, then a conservation approach is to subtract this value from the excess heat registered in the hydrogen cell. The result of this subtraction is shown by the dashed green trace in the cell 1 graph. This reduces the inferred excess heat in the hydrogen from 1 W to 0.8W up to about 950 hours and to 0.7W thereafter. Using this adjusted power, 6.3% more power is measured than is input.

However, note that the pressure during these measurements is 1.24, about 20% higher than the pressure in the cells during the pressure calibration. If the 1-bar calibration data points for cell 2 are adjusted for this higher pressure and refit to create a 1.2-bar cell 2 algorithm [see Appendix E] and this algorithm is used to calculate the excess power in the nitrogen cell, the solid red trace in the lower graph results. This line, except for the periodic temperature error, lies near zero excess power. Using this line to adjust the hydrogen excess power curve downward an excess power of 1 W up to about 950 hours and to 0.9 W thereafter is obtained. Using this adjusted power, 7.5% more power is measured than is input. This latter correction is judged to be the most accurate. To a much lesser extent, a variable scaling correction should be applied to the cell 1 excess power trace between 280 hours and 500 hours.

Power to cell 1 was reduced by 0.1 W in two steps at 885 and 935 hours, which reduced the temperature of the cell interior 2°C, dropping the excess power by 100 mW. Commanding a power increase at 1180 hours to 13.0 W (0.3W above the previous 12.7W) raised the temperature to 297°C but recovers only 40 mW of this lost 100 mW of excess power. The same 300 mW increase in cell 2 did not similarly affect its excess heat traces. Returning the input power to cell 1 at 1275 hours created a large decrease in excess power as discussed below.

The time integration of the solid (dark) green excess power trace in the upper graph yields the excess energy. This integration was performed from 280 hours to 1275 hours and then normalized by the mass of the sample to yield a value of specific energy. Normalizing to the 20 gram mass of the ZrO_2NiPd sample yields a specific energy of 173 MJ/kg whereas assuming that the active element is the 5.44g of Ni+Pd [Appendix F] yields a specific energy of 635 MJ/kg. Normalized to the Pd would yield a specific energy 10x that of the Ni specific energy value. For comparison, methane fuel has a specific energy of 55.5 MJ/kg, the highest value for any hydrocarbon fuel; hydrogen compressed to a pressure of 700 bar has a value of 142 MJ/kg, the highest value for any chemical fuel. [17] These chemical values are somewhat arbitrary as they require an oxidizer, which is not included in the mass.

4.5 Power Down Period

The termination sequence of the experiment began after 1275 hours and is shown in Figure 4.8. This time was chosen for practical considerations and not due to any observed abatement of excess power. This sequence was complete at 1610 hours, a period of 14 days. The traces in these graphs are the same as those identified in Figure 4.7.

It is immediately apparent that the excess power traces in the hydrogen (upper) graph are noisy. This problem began as the power to the cell was reduced. This may be due to a malfunction in the regulated output of the hydrogen cell power supply as can be seen in the blue power trace. Even with this noisy data, it is clear that a small (12°C) change in temperature decreases the excess power by nearly a factor of 2. Increasing the temperature 5°C at 1326 hours did not increase the excess power. Stepping down in input power and temperature produces a credible decrease in excess power (solid green trace) as calculated by subtracting the scaled N_2 excess power. The last temperature step decrease of 150°C reduced the excess power of 180 mW to zero at room temperature.

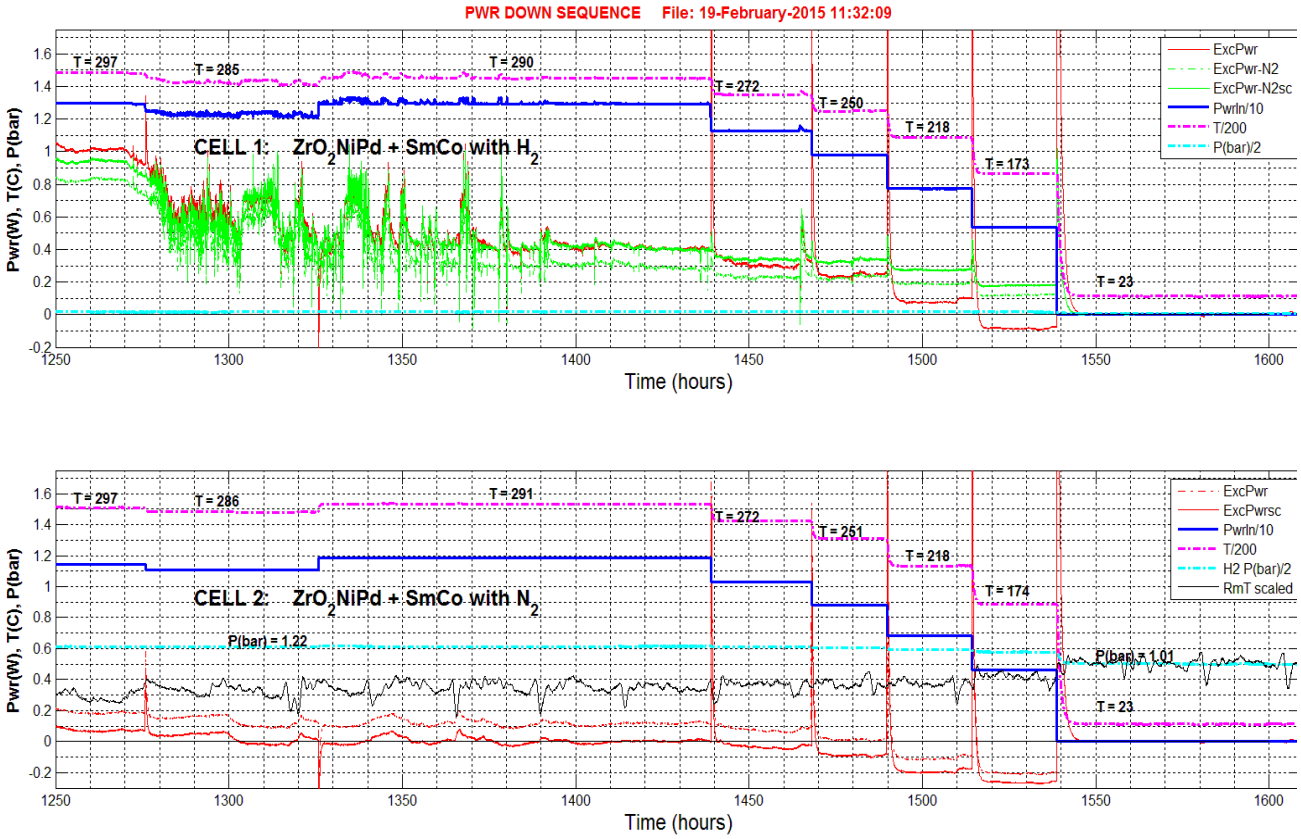

Figure 4.8 Data from the termination sequence of the experiment.

The data at temperatures 23°C <T ≤ 250°C in the nitrogen (lower) graph produce negative excess powers (solid red trace). The -300 mW value at 1525 hours is too large to be ascribed to a pressure-induced error in the calibration curve or measurement error in the input power. It is more likely due to a temperature lower than that anticipated by the calibration curve; i.e., a cooling not accounted for in the calibration measurements. However, at room temperature, the algorithm does produce zero excess power. During this final interval, the room temperature increases 1°C and in the final temperature step the nitrogen pressure drops 20%. The scaled 1.2 bar calibration curve is used throughout all these intervals.

5. Discussion and Conclusion

A shortcoming of this work is the method chosen to measure the power generated by the sample. Power was inferred from a temperature measured by thermocouples imbedded in the sample. This inference was made using algorithms generated by applying known powers to the fully configured sample chamber and measuring the resultant temperature from a thermocouple. It is prudent to quantitatively examine the error in this method.

Sources of error in measuring the excess power using this method include:

1. Inaccurate input power measurements.
2. Systematic errors in the thermocouple temperature measurement.
    a. Reference junction error.
    b. Error due to temperature gradient in sample.
    c. Exothermic or endothermic chemical reaction between thermocouple and the sample/gas.
3. Errors of the calibration algorithm.
    a. Uncorrected variation with pressure.
    b. Uncorrected variation with temperature
    c. Variation of thermal conductivity with gas composition.
    d. Time constant errors.

Error in the excess power measurement due to items 1 and 2 are estimated by an error propagation calculation. Assuming that the principal source of error is temperature, we can estimate the error in the power. If the power, P, as a function of temperature, T, is given by Eq. 1 in Section 4.1. then error in the power, σ_P, is [18]

$$\sigma_P = \sigma_T \left[\frac{\partial P}{\partial T}\right] \tag{2}$$

or

$$\sigma_P = \sigma_T (3aT^2 + 2bT + c) \tag{3}$$

where a, b, and c are the coefficients of the cubic, quadratic, and linear terms in Eq. 1.

For T = 300°C, taking the coefficients from the hydrogen vacuum fit and estimating the temperature error to be 0.5°C, we find propagated error in the inferred power in the hydrogen cell is $\sigma_{P_{H_2}} = 0.049$ W.

The excess power is $P_{ex} = P_{H2} - P_{in}$ so

$$\sigma_{P_{ex}}^2 = \sigma_{P_{tot}}^2 + \sigma_{P_{in}}^2 \tag{4}$$

Accordingly, $\sigma_{P_{ex}} = 0.049$ W for a 10 mW error in the measured input power (the measured error in the input is less than half this assumed value). For an excess power of 1 W, this is an absolute error of 5% in the power and the integrated excess energy.

Regarding error 2c, type K thermocouples have a well-known inaccuracy if operated in a reducing (i.e., hydrogen) atmosphere. The hydrogen chemically reacts with the thermocouple metals resulting in what has been dubbed "green rot." However, this phenomenon only occurs at temperature above 800°C and results in temperature readings lower than actual (for example, see Ref. [20]). The maximum temperature used in this work was near 300°C and if even this were an issue the result would be an underestimate of the measured excess energy.

Systematic errors in 3a and 3b were considered in the data processing as discussed in Section 4.4. These errors are judged to be on the order of 0.05 W based on the renormalized curve of the nitrogen cell. In the analysis the excess power is reduced by this amount to conservatively account for this error. Item 3c could be a concern as the cell calibrations were done with nitrogen and the thermal conductivity of nitrogen gas and hydrogen gas differ by a factor of nearly seven at high temperatures (see Appendix C and Ref. [19]). However, since the 0 bar pressure calibration was used for the calculation of the power in the hydrogen cell, this is not an issue. In the future it may be prudent to use helium (which has a thermal conductivity closer to that of H_2, see Appendix C) for the calibration and in the reference cell.

Even if the power is inferred from the temperature exactly, all sources of mechanical and chemical energy sources must be understood before an anomalous value (if any) can be assigned. Other sources of energy:

- PV work in pressurizing the cell
- Heat adsorption exothermic energy released

These sources were discussed in Section 4.2 and are not significant.

In summary, for the 950 hour (40 day) integration period: N_2 cell excess energy is 0.12 MJ; the difference between the hydrogen cell and nitrogen cell excess energy is 3.5 MJ (±5%). The H_2 cell excess power (less N_2 excess power) was 7.5% of input power. The H_2 cell specific energy (less the N_2 excess energy) = **173 MJ/kg** (20 gm ZrO_2NiPd) or H_2 cell specific energy (N_2 corrected) = **635 MJ/kg** (5.4gm NiPd). For reference, methane (hydrocarbon fuel with highest specific energy) = 55.5 MJ/kg, and H_2 highly compressed to 700 bar (highest known chemical specific energy) = 142 MJ/kg.

For the 300-hour power down sequence the H_2 cell excess power traces values appear credible. There is some evidence of excess power abatement. The low temperature N_2-cell excess-power traces are not completely understood.

The results presented here indicate a source of heat energy was measured that is not chemical in origin. This measurement and conclusion are in general agreement with those of Arata and Zhang [4] and Ahern [5]. Given the importance a source of high specific energy has for space technology, this work indicates that additional research should be pursued. If future work is better funded, calorimetry should be used instead of thermometry to measure the heat power.

6. References

1. The 23 March 1989 televised press conference can be viewed at links found at http://news.newenergytimes.net/ and currently at https://www.youtube.com/watch?v=6CfHaeQo6oU
2. M. C .H. McKubre, F. L. Tanzella, and V. Violante, "What is needed in LENR/FPE studies," J. Condensed Matter Nucl. Sci **8**, 187-197 (2012).
3. S. Focardi, R. Habel, and F. Piantelli, Il Nuovo Cimento Note Brevi Vol. 107 A, N. 1 (1994). Campari, E., Focardi, S., Gabbani, V., Montalbano, V., Piantelli, F., Veronesi, S., "Overview of H-Ni Systems: Old Experiments and New Setup," 5th Asti Workshop on Anomalies in Hydrogen- / Deuterium-Loaded Metals, Asti, Italy, (2004).
4. Y. Arata and Y. C. Zhang, 'Formation of Condensed Metallic Deuterium Lattice and Nuclear Fusion," Proc. Jpn. Acad. Ser. B, 2002 78(Ser. B), p. 57 2.
5. B. Ahern, "Program on Technology Innovation: Assessment of Novel Energy Production Mechanisms in a Nanoscale Metal Lattice," EPRI Report 1025575, Technical Update, August 2012.
6. M. Swartz, G. Verner, J. Tolleson, L. Wright, R. Goldbaum, and P. Hagelstein, "Amplification and Restoration of Energy Gain Using Fractionated Magnetic Fields on ZrO_2-PdD Nanostructured Components," J. Condensed Matter Nucl. Sci. **15**, 66-80 (2015).
7. L. L. Jones, Materials Preparation Center (MPC), 121 Metals Development Building, Ames Laboratory, Ames, IA 50011-3020, jonesll@ameslab.gov.
8. Spex SamplePrep 65 Liberty St., Metuchen, NJ 08840, USA.
9. Aremco Products Inc., 707 Executive Blvd., Valley Cottage, NY 10989,Tel: +1 (845) 268 0039, Fax: +1 (845) 268 0041, http://www.aremco.com.
10. AlphaWire PIF-240-12 uncoated fiberglass sleeving, heat annealed braided fiberglass; temperature range -60°C – 648° C, http://www.alphawire.com/Home/Products/TubingAccessories/FIT-Wire-Management/Sleeving/PIF24012.
11. OMEGA Engineering, Inc., One Omega Drive. P.O. Box 4047, Stamford, Connecticut 06907-0047.
12. Transducers Direct, 12115 Ellington Court, Cincinnati, Ohio 45249. Part no. TD1000CCGV28503D002X, IBS ADE831 and ADE832, Cal Due Date 3/1/15)
13. D. Severin, K. Sarakinos, O. Kappertz, A. Pflug, and M. Wuttig, J. Appl. Phys **103**, 083306, 2008.
14. M. Johansson, E. Skulason, G. Nielsen, S. Murphy, R. M. Nielsen, I. Chorkendorff, "Hydrogen adsorption on palladium and palladium hydride at 1 bar," *Surface Science* **604**, 718-729 (2010).
15. D. J. Nagel, "Lattice-enabled nuclear reactions in the nickel and hydrogen gas system," CurrentScience, 108, 646 (2015) citing http://www.rebresearch.com/H2sol2.htm.
16. R. Wiswall, "Hydrogen Storage in Metal," Chapter 5 in *Hydrogen in Metals II*, Topics in Applied Physics Vol. 29, G. Alefeld and J. Volkl, (*eds*.) Springer-Verlag, New York, 1978.
17. http://en.wikipedia.org/wiki/Energy_density
18. P. R. Bevington, *Data Reduction and Error and Analysis for the Physical Sciences*, McGraw-Hill, New York, 1969.
19. S. C. Saxena, "Transport properties of Gases and Gaseous Mixtures at High Temperatures," High Temp. Sci. 3, 168-188 (1971).
20. http://www.transcat.com/calibration-resources/application-notes/thermocouples/)
21. O. Dmitriyeva, G. Moddel, R. Cantwell, M. McConnell, "Using Bakeout to Eliminate Heat from H/D Exchange During Hydrogen Isotope Loading of Pd-impregnated Alumina Powder," J. Condensed Matter Nucl. Sci 12 (2013) 13-17.
22. Magnet Sales and Manufacturing Inc.: High Performance Permanent Magnets 7, http://www.magnetsales.com. Grade 26 SmCo sintered magnet, Part # 26DRE4816, Magnetic Sales, Culver City, 310 391-7213, Alan Yamamoto.
23. S. C. Saxena, "Transport properties of Gases and Gaseous Mixtures at High Temperatures," High Temp. Sci. **3**, 168-188 (1971).
24. http://www.electronics-cooling.com/2002/11/the-thermal-conductivity-of-air-at-reduced-pressures-and-length-scales.

Appendix A. The First Experiment Trial

This first trial served primarily as a learning vehicle for developing and testing an experimental protocol. A secondary objective was the observation of excess heat of non-chemical origin. A tertiary goal was to see the effect, if any, of magnetic particles in the active material (see Appendix B). Thus the two cells in this experiment were identical except for the addition of magnetic particles in the second cell. The desired test plan for first run comprised seven steps.

1. Load 10 grams of 1 – 3 micron ZrO_2NiPd powder to be tested in cell 1.
2. Load 10 grams of 1 – 3 micron ZrO_2NiPd powder mixed with 10 gm of SmCo powder in cell 2.
3. Vacuum bake both cells at 390°C for 35 hours to remove water.
4. Pressurize cells 1 and 2 in parallel with D_2 at 7 bar (100 psia) at 22°C to load micro-powder with deuterium. After pressure drops, recharge with D_2 until fully loaded (up to 10X in an hour).
5. Equalized D_2 pressure in both cells.
6. Heat cells individually to 280°C recording four temperatures, pressures, input power.
7. Record data at 30s intervals for duration of experiment (days/weeks).

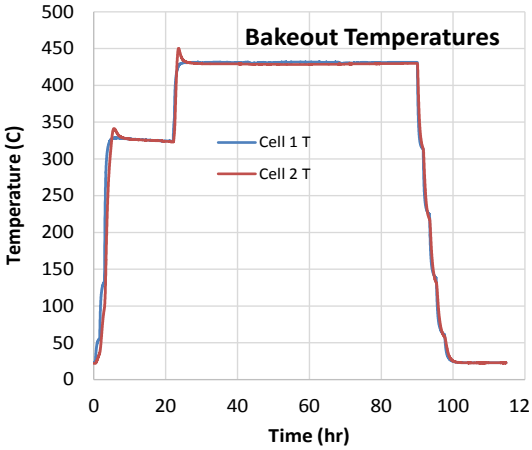

Figure A.1 First bakeout of samples under vacuum.

This desired protocol could not be followed due to an unusual pressure response during the first D_2 loading. This led to the vacuum bakeout being done twice at higher than the desired temperature and to an anomalous pressure behavior during the loading of the D_2 gas.

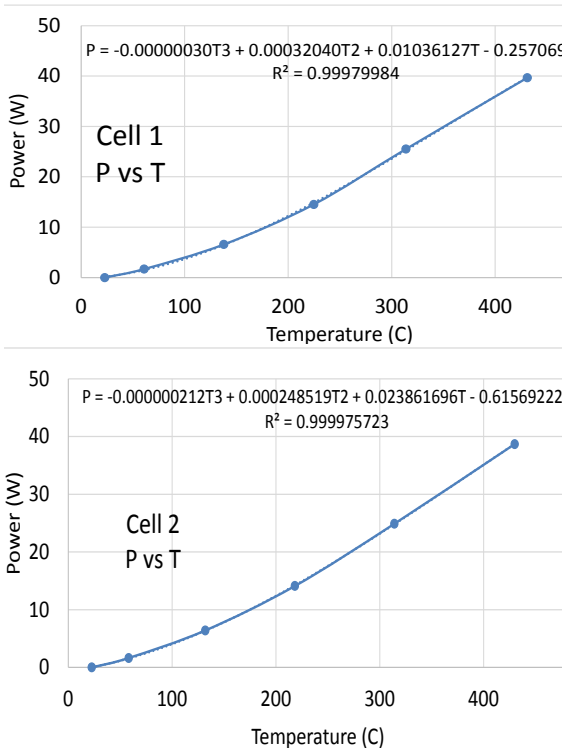

Figure A.2 Calibration fits for two cells.

The time sequence used is given in Figures A.1 and A.3. Samples were loaded into the two cells and baked at 430°C for 60+ hours to remove H_2O as shown in Figure A.1. Previous studies indicate that a bakeout at 390°C for 35 hours was shown to be sufficient to eliminate heat from H/D exchange reactions from light water (H_2O) trapped in the samples. [21] The calibration data were then acquired by raising the samples from room temperature (23°C) to 430°C in five steps, recording the input power to each cell with the cells under vacuum. The resulting data were fit to a third order polynomial to create algorithms to be used to infer the power from a temperature measurement. Subsequently the cells were elevated in temperature to check that the inferred power from

the temperature measured equaled the input power. This check was done both with the cell under vacuum and pressured with about 0.5 bar (400 Torr) of N_2. The calibration curves are given in Figure A.2. Note that the cell response is approximately 8.5°C per Watt of input power. Performing the calibration with the cells in the exact configuration (mass, thermocouple placement, etc.) was judged as the most reliable method to infer power from temperature.

Subsequently, the cells were evacuated and filled with 2.5 bar (36 psia) of D_2. The pressure initially dropped to 2.3 bar (33 psia) during the first hour but the pressure increased to 3.0 bar (43 psia) overnight. After this puzzling behavior it was decided to evacuate the cells again and bake them overnight at 225°C. After the overnight bakeout, the cells were cooled to room temperature and pressurized with 2.5 bar (36 psia) of deuterium. After 4 hours, the pressure was reduced to about 1 bar and power was applied to bring the temperature of the cells to near 280°C, thus beginning the experiment.

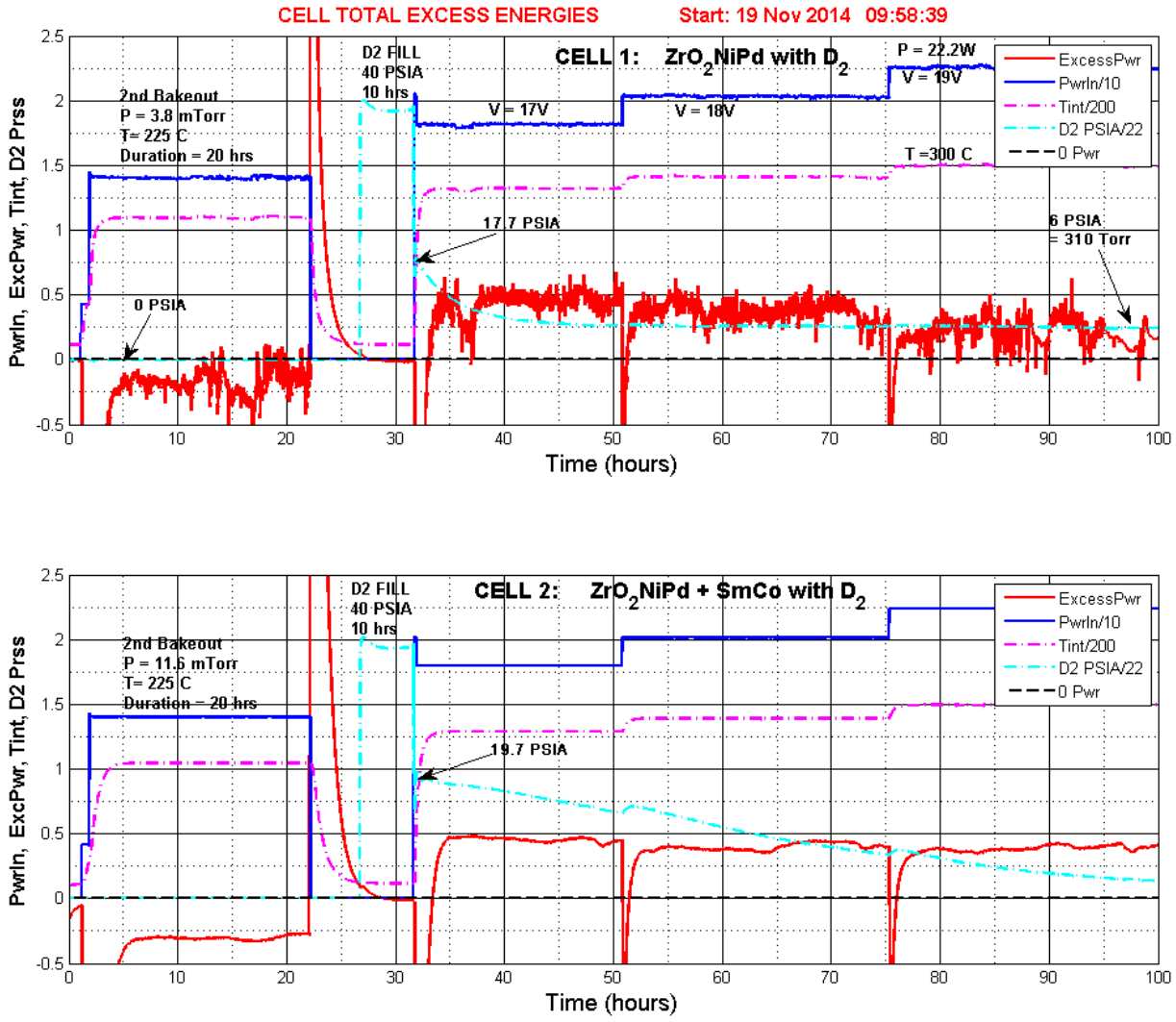

Figure A.3 First 100 hours of first experiment showing excess power, power in, temperature and pressure.

Figure A.3 shows the first 100 hours of the experimental run. This figure highlights the second bakeout and D_2 gas fill and the initial heating of the cell designed to trigger the reaction. In this plot there are four data traces; each are read on the left axis with the scaling factors given in the figure legend. The top graph displays the data from cell 1 that contained only the ZrO_2NiPd material; the bottom graph plots the data from cell 2, which contains the identical material as that in cell 1 plus the magnetic particles. The heavy

blue curve is the power input to the cell divided by 10. Note that the power supplies are operated in constant voltage mode with same voltage going to each cell. Because of a small difference in the length of the heater wires, the power is slightly different for the two cells for the same input voltage. The temperature in Celsius divided by 200 is given by the dashed pink line. Pressure of the deuterium gas in PSIA divided by 22 is given the blue-green dashed line. Finally, the excess power is plotted using a solid red line. This power is the difference between the power inferred from the measured temperature using the calibration curve (Figure A.2) and the input power.

It is interesting to note the behavior of the pressure. In cell 1, after lowering the pressure to about 1.2 bar (18 psia) and closing the cell valve, the pressure decreases for about 10 hours as the cell is heated to 350°C to a constant value of about 0.4 bar (6 psia). The behavior of the D_2 pressure in cell 2 is quite different. It was closed at a similar starting pressure but it decreased to near zero over a much greater time (>200 hours as can be seen in Figure A.4). It is not known whether the different pressure behavior between the two cells is due to a leak in the vacuum jacket in cell 2 or the characteristics of the SmCo particles.

Figure A.4 shows the entire data set from experiment 1, a period of 550 hours or nearly 23 days. All data traces are the same as those identified in Figure A.3. The heating of the cells to trigger the reaction began at hour 31.5. The large "spikes" in the excess power curves occur whenever the power supplied to the cell is changed and are due to the time required for the cell to reach the equilibrium temperature used in the calibration function. These excursions are positive when increasing the power to the cells and negative when decreasing the power to the cells. The excess power is correct only after equilibrium is reached. All changes to the input power were made at the same time with identical voltages applied to the heater coils. The total excess energy is calculated by integrating the excess power curve with time starting at hour 33.6.

There are obvious and significant differences in the excess power curves between the two cells. First, the time response is much faster in cell 1. This is likely to due to the smaller thermal mass of the sample in cell 1 and possibly to different thermocouple placement in the two cells. If the thermocouple were touching the interior stainless steel wall of cell 2, the temperature variations would be much slower than that of cell 1 if the cell 1 thermocouple were isolated in the sample. Although this would affect the time to equilibrium it should not affect the inferred power because it would be in the same position during the calibrations runs. Second, the excess power was significantly greater in the cell with the magnetic particles. The integrated specific excess energy for cell 1 (assuming the relevant mass is 10 grams) is 21 MJ/kg whereas for cell 2 it is 69 MJ/kg. Note that if the relevant mass is considered just the nickel and palladium then the specific energy is about three times these values. As noted in Section 4, the most energy dense hydrocarbon is methane at 55.5 MJ/kg. [17]

The most interesting difference between the two cells is the behavior of the excess energy as the temperature is lowered at 330 hours into the run. For most of the experiment the cell temperature was held near a temperature of 300°C. For cell 1, no significant change in the excess power was observed when the temperature was lowered from 300°C to 225°C in three steps. However, in cell 2, the excess power increased for each of these steps. When the temperature was lowered to 130°C, the excess power in cell 1 decreased to near 0 whereas the excess power in cell 2 increased to its highest value. Lowering the temperature to 50°C, the excess power in cell 2 was still 0.25 W. At room temperature, excess power of both cells was zero. For cell 1, the power always decreased with decreasing temperature and was zero at 130°C. For all these experiments the maximum excess power was 0.6 W (a temperature change of 5°C) in cell 2 while heating with 6.3 W. For the case of the magnet-mixture, the excess power continued until the temperature was lowered to room temperature, a period of about 18 days.

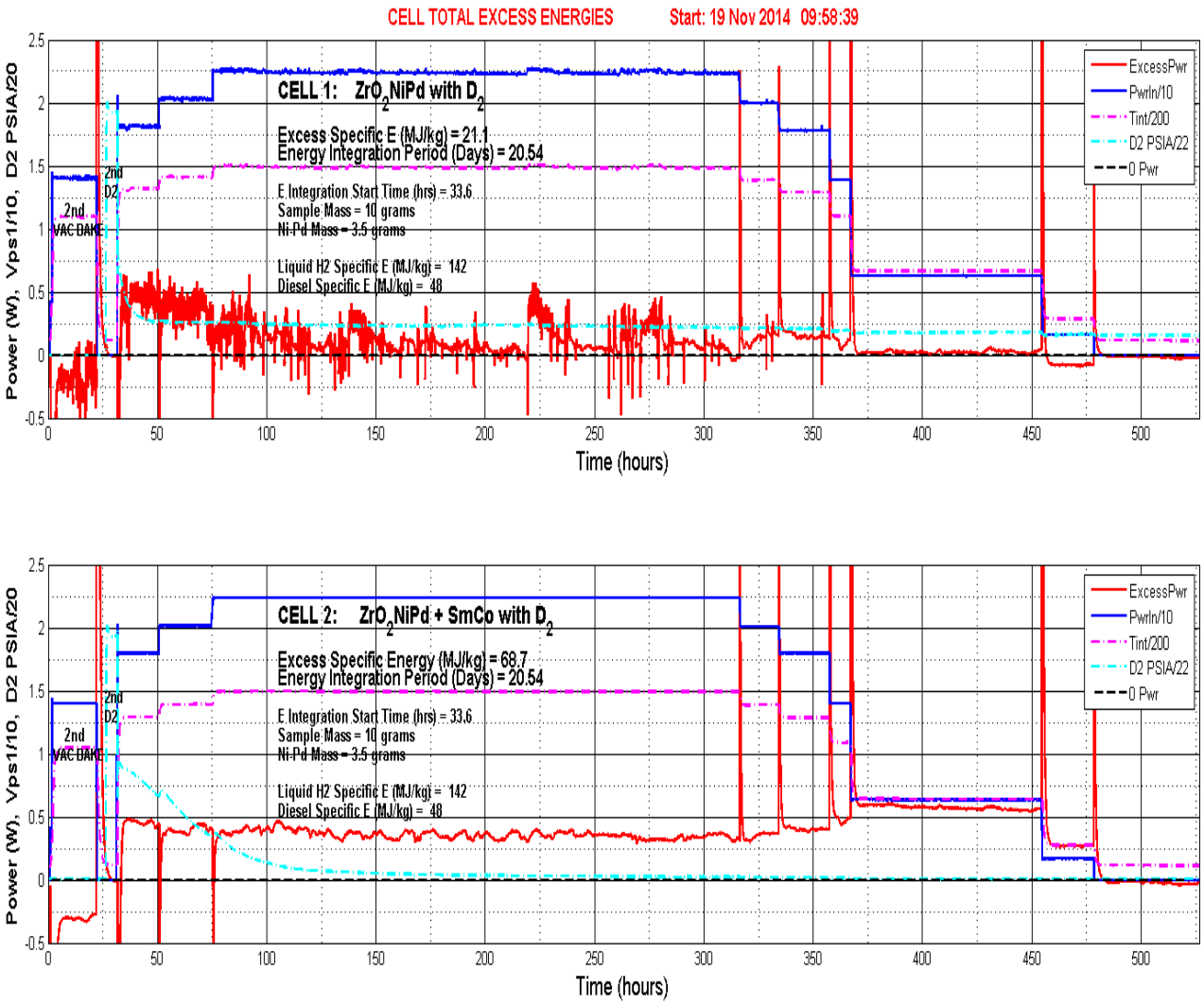

Figure A.4. Entire data set from first experiment.

As previously mentioned, several investigators have noted increased excess energy in the presence of a magnetic field (for example, see Ref. [6]). These data tentatively support those observations. The increase in excess energy as the temperature is lowered may be due to an increasing magnetic field as the temperature is lowered, as discussed in Appendix B. However, based on the measurements presented in Appendix B, only an increase of about 15% in the magnetic field is expected by lowering the temperature from 300°C to 23°C.

The observation of excess heat in this first experiment was encouraging. However, the data cannot be considered definitive. Major short comings include data taken at a pressure different than used to generate the calibration curves; bare thermocouples that chemically react with test materials; and unknown positions of the thermocouples in the cells (touching walls or not in contact with test material). These shortcomings were corrected in the second experiment. Based on this work, the following changes were made for the principal experimental trial:

- Better thermally isolated cells with less heat capacity and welded internal fittings were used.
- Sample was baked out below 350°C.
- Two interior thermocouples were used.

- The interior thermocouples were shielded from the sample material.
- A manual readout gauge with 0-70 psia (5 bar) range was installed.
- 0-285 psia (20 bar) pressure transducers were replaced with 0-90 psia (6 bar) transducers.
- The mass of the active material in each cell was increased to 20 grams and enough magnetic particles (6 grams of SmCo) to fill the remainder of the cell volume.
- Samples were ground to < 1 micron diameter.
- H_2 gas was used instead of D_2.
- Real-time temperature and pressure digital readouts were written into DAQ software.
- Excess power plot was added to DAQ real-time graph.
- X-ray tomography was used to observe the cell packing and thermocouple positions.

Appendix B. Germaine Properties of Rare Earth Magnets

There have been many reports of evidence that a magnetic field can enhance the AHE. Perhaps the most quantitative, available, and relevant to NiPd nanoparticles in a ZrO_2 matrix is Ref. [6]. To explore this, the second cell was filled with a mixture of approximately equal weights of a milled SmCo 2-17 magnet and the ZrO_2NiPd sample described above.

Although the magnetic field strength of NdFeB magnets is higher than that of SmCo 2-17 magnets, the working temperature of the SmCo magnets is higher than that of the Nd magnets. The working temperature for most NdFeB magnets is usually below 150^o C (even though the Curie temperature is much higher). The magnetic field decreases above the working temperature. Furthermore, NdFeB magnets oxide quickly and usually are coated with Nickle or Tin. The oxidized particles have diminished magnetic properties. At the temperatures above 150°C, 2Sm-17Co magnets usually will have a higher magnetic field than NdFeB magnets. A comparison of the B-field strength of SmCo and NdFe magnets taken from the supplier's catalogue is shown in Figure B.1, indicating a superior performance of the SmCo magnet with increasing temperature.

Table B.1. Magnetic Properties of Two Selected Magnets*

Material Grade	B_r (Gauss)	H_c Oersted	H_d Oersted	BH_{max} MGOe	Recoll Perm.	Slope BH_{max}	Curie T(ºC)	Max Op T(ºC)	T Coeff DBr/Br/ºC(%)
SmCo 26	10,500	9,200	10,000	26	1.08	1.0	825	550	-0.03
NdFeB28	10,800	10,100	17,000	28	1.09	1.0	310	150	-0.09

*Page 23 Magnetic Sales Catalog [22].

SmCo 27H

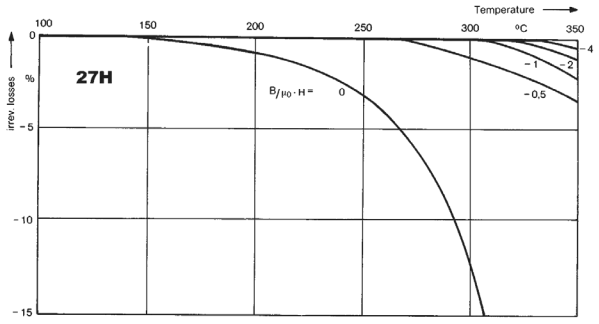

NdFeB 32SH

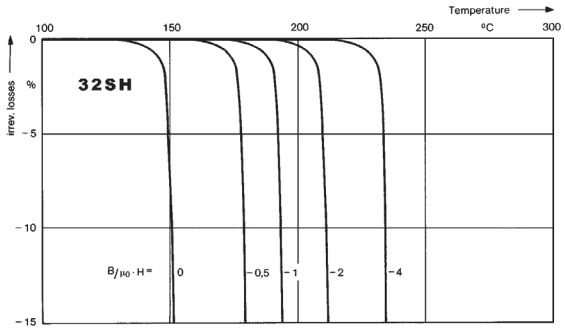

Figure B.1. Temperature Properties of selected SmCo and NdFeB magnetics from page 29 of Magnetic Sales Catalog [22].

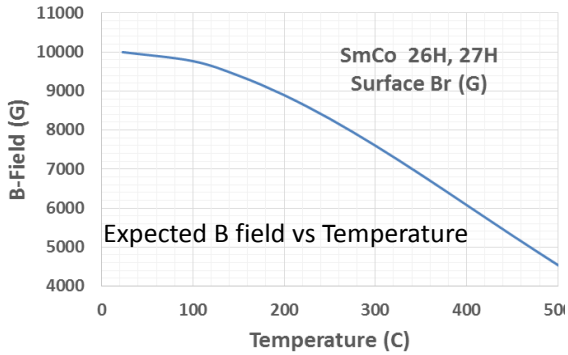

Figure B.2. Expected temperature dependence of purchased magnets from catalogue specifications.

Based on this analysis, Grade 26 SmCo disk magnets of 3/4" diameter X 0.25 thick magnets where obtained [22] and crushed in a mortar and pestle. The quoted field strength and the T coefficient for the magnet used in the experiment is given in Table B.1 and the expected field as a function of temperature is shown in Figure B.2. According to this plot, the maximum field strength is 1T at room temperature and decreases to 50% of this value at 500°C.

However, measuring the performance of this magnet in our laboratory found the maximum B-field at the surface of the magnet to be 2600 gauss and that it decreased to 1650 gauss at 450°C, a drop of about 35% (Figure B.3). Cooling the magnet to room temperature, the surface field returned only to 2000 gauss also shown in Figure B.3. Reheating the magnetic to 450°C, the field again reduced to 1650 gauss, a drop of 17%.

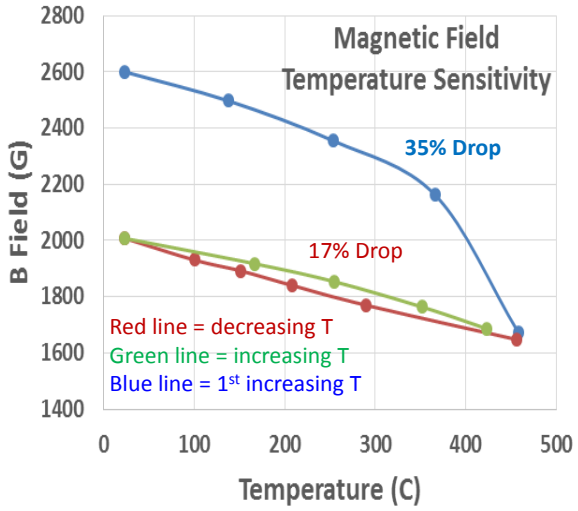

Figure B3. Actual (measured) temperature dependence of purchased magnets.

Appendix C. Heat Capacity and Thermal Conductivity of N_2, H_2, and D_2

Table C.1 Low Temperature Properties of N_2, H_2, and D_2

Nitrogen Gas - N2				Hydrogen Gas - H2			per mole		Deuterium Gas D2				
T (K)	kJ/kg/K	kJ/mole/K		T (K)	kJ/kg/K	kJ/mole/K	c(H2/N2)		T (K)	cal/mole/K	kJ/kgK	kJ/mole/K	c (H2/D2)
175	1.039	0.029		175	13.12	0.026	0.91						
200	1.039	0.029		200	13.53	0.027	0.94		190	6.983	7.3042	0.0294	0.9269
225	1.039	0.029		225	13.83	0.028	0.96		220	6.975	7.2959	0.0294	0.9485
250	1.039	0.029		250	14.05	0.028	0.97		260	6.975	7.2959	0.0294	0.9636
275	1.039	0.029		275	14.2	0.029	0.98						
300	1.04	0.029		300	14.31	0.029	0.99		300	6.977	7.2979	0.0294	0.9811
325	1.04	0.029		325	14.38	0.029	1.00						
350	1.041	0.029		350	14.43	0.029	1.00						
375	1.042	0.029		375	14.46	0.029	1.00		J. Chem Phys 1, 137 (1933)				
400	1.044	0.029		400	14.48	0.029	1.00						
450	1.049	0.029		450	14.5	0.029	0.99		amu				
500	1.056	0.030		500	14.51	0.029	0.99		H	1.0078			
550	1.065	0.030		550	14.53	0.029	0.98		D	2.0141			
600	1.075	0.030		600	14.55	0.029	0.97		N	14.003			
650	1.086	0.030		650	14.57	0.029	0.97						
700	1.098	0.031		700	14.6	0.029	0.96						
750	1.11	0.031		750	14.65	0.030	0.95		since N (mole) = pV/kT then a given pressure will have				
800	1.122	0.031		800	14.71	0.030	0.94		same heat capacity so can use any gas as long as				
850	1.134	0.032		850	14.77	0.030	0.94		heat transfer is same				
900	1.146	0.032		900	14.83	0.030	0.93						
950	1.157	0.032		950	14.9	0.030	0.93						
1000	1.167	0.033		1000	14.98	0.030	0.92						
1050	1.177	0.033		1050	15.06	0.030	0.92						
1100	1.187	0.033		1100	15.15	0.031	0.92						
1150	1.196	0.033		1150	15.25	0.031	0.92						
1200	1.204	0.034		1200	15.34	0.031	0.92						
1250	1.212	0.034		1250	15.44	0.031	0.92						
1300	1.219	0.034		1300	15.54	0.031	0.92						
1350	1.226	0.034		1350	15.65	0.032	0.92						
1400	1.232	0.035		1400	15.77	0.032	0.92						
1500	1.244	0.035		1500	16.02	0.032	0.93						
1600	1.254	0.035		1600	16.23	0.033	0.93						
1700	1.263	0.035		1700	16.44	0.033	0.94						
1800	1.271	0.036		1800	16.64	0.034	0.94						
1900	1.278	0.036		1900	16.83	0.034	0.95						
2000	1.284	0.036		2000	17.01	0.034	0.95						

http://www.engineeringtoolbox.com/nitrogen-d_977.html

Table C.2 High Temperature thermal Conductivity of N_2, H_2, and D_2 [23]

(k in W/m/K)

Temperature (K)	k (H_2)	k (D_2)	k (He)	k (N_2)
350	0.205	0.154	0.170	0.0311
400	0.224	0.166	0.184	0.0335
500	0.261	0.192	0.212	0.0383
600	0.298	0.217	0.240	0.0431
700	0.334	0.243	0.269	0.0478

Appendix D. Room and Cell Temperature Difference Data

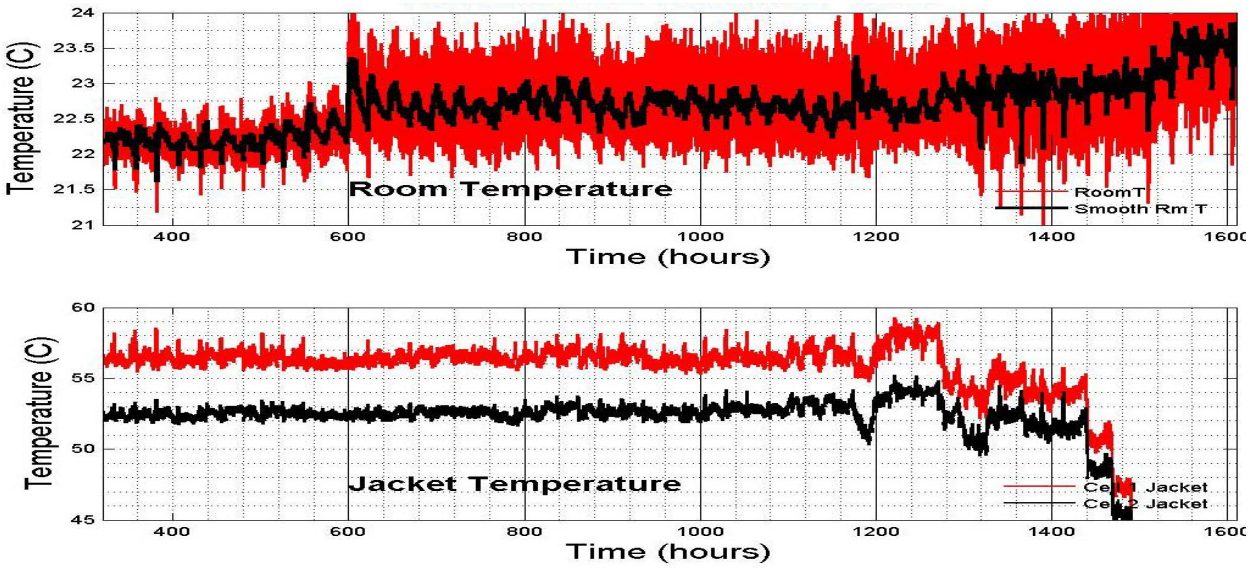

Figure D.1 Room Temperature and Vacuum Jacket Temperatures.

The room temperature thermocouple was a fine wire thermocouple suspended in air yielding a small time constant. The jacket thermocouple was fixed to the stainless steel jacket with a significant thermal mass.

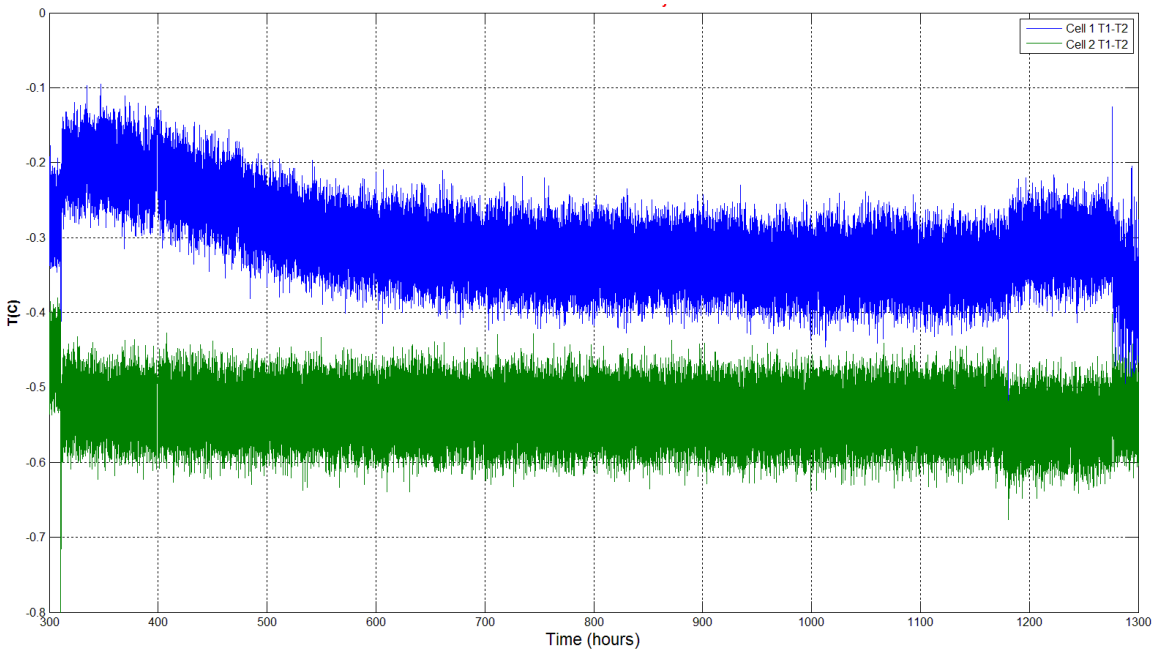

Figure D.2 Temperature difference between cell interior thermocouples during energy integration period.

Appendix E. Scaled Nitrogen Cell Calibration

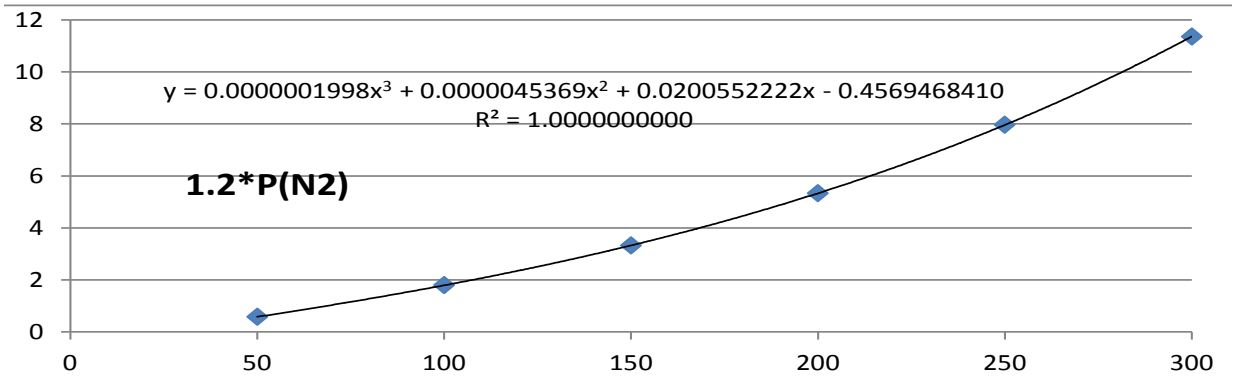

Figure E.1 Calibration Fit Scaling 1.0 bar Data to 1.2 bar.

The difference values between the predicted vacuum and 1 bar polynomial fit values scaled by a factor of 1.2 are given in Table E.1.

Table E.1 Scaling of Nitrogen Calibration 1-bar Values by 20%

Values predicted by polynomial Fit				
	Cell #2 Vac vs N2			
T	P (Vac)	P (N2)	Diff	1.2Diff
50	0.613049	0.58728	0.025769	0.704736
100	1.917931	1.814408	0.103522	2.17729
150	3.594748	3.37213	0.222619	4.046556
200	5.762902	5.405194	0.357709	6.486232
250	8.541793	8.058351	0.483442	9.670021
300	12.05082	11.47635	0.574469	13.77162

Appendix F. Calculation of Elemental Mass of the Principal Experimental Trial

As noted in section 2, the base metallic material, was prepared by Ames Laboratory [7] by arc melting a 90 gram mixture of 65wt% Zr 32wt% Ni 3wt% Pd using 99.95% purity elements. These were delivered in a series of nine envelopes, each marked with the mass of the metal used to charge the ribbon fabricator instrument. After receiving, the ribbon in each envelop was weighted. The results for the samples used in the principal experimental trial are given in Table F.1

Table F1 Ribbon Mass

Envelope	Charge Mass (g)	Ribbon Mass (g)
5	9.38	8.745
6	9.59	8.930
7	9.07	4.385
8	8.49	3.850
8+7 Wheel Material	--	8.190

The total of this ribbon material = 34.10 g and was placed in a furnace and heated at 440^{o}C for 28 hours creating a ZrO_2 matrix imbedded with nanometer sized islands of Ni and Pd [5]. This brittle material was ground in a mortar and pestle and passed through a No. 35 mesh (0.5 mm). The mesh separated the ductile ribbon which did not grind from the oxide. Both components were weighted yielding 43.65 g of oxide and 0.20 g of ribbon. Therefore the masses of the metallic elements in the oxide can be calculated from the ribbon material in the oxide; i.e., 34.1g – 0.20g = 33.90g:

Metal in Oxide: 0.65 x 33.90g Zr; 0.32 x 33.90g Ni; 0.03 x 33.90g Pd;

= 22.03g Zr; 10.85g Ni 1.02 g Pd.

Thus the oxygen mass is 43.65g – 33.90g = 9.75g and the percentages of the materials in the oxide are given in Table F.2

Table F2 Elemental Composition

Element	Mass (g)	% Mass	Mass in Cell (g)	At Wt (amu)	Moles in Cell
Zr	22.03	50.5	10.10	91.224	0.111
Ni	10.85	24.9	4.98	58.6934	0.0849
Pd	1.02	2.03	0.46	106.42	4.32×10^{-3}
O	9.75	22.3	4.46	15.9994	0.279
Total	43.65 g	100%	20.0g	--	--
Adsorbed H_2	--	--	--	2.0	2.7×10^{-3}

Six grams of SmCo particles were added to the 20 g sample of oxide material in each cell. The total of the Ni and Pd active metal is 5.44 g. The mole ratio of Ni:Pd is 19.6:1.

Appendix G. Calculation of H_2 Exothermic Loading Energy

The energy produced during hydrogen loading is calculated by converting the temperature rise to power using the 1 bar calibration curve for cell 1 shown in Figure 4.5 and integrating that power over time (see Figure G.1). Assuming that 100 kJ/mole of energy is released when absorbed by Pd [14] implies 0.011 moles of H_2 are absorbed by Pd.

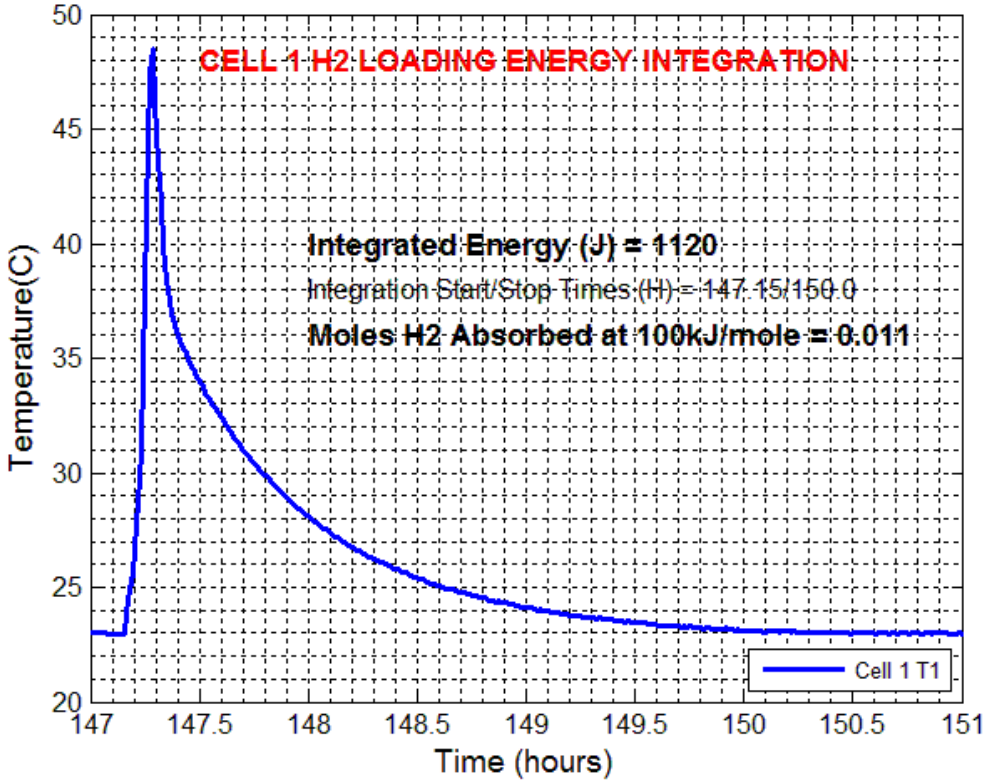

Figure G.1 Integration of hydrogen loading power to obtain loading energy.

Appendix H. Cell Pressure History

Table H.1 Cell Pressure History

Condition	Cell 1	Cell 2	Comments
N_2 Calibration	4 mbar/h (0.4%)	0.5 mbar/h (0.05%)	
Bake Out	22mT (330°C) ---> 4 mT 340°C)		42 hours
Gas Loading	137 mbar/h		4.5 bar 22°C (ΔT H_2 = +25°C)
Gas Loading	187 mbar/h	15 mbar/h	4.5 bar 22°C
Gas Loading	105 mbar/h		4.5 bar 22°C

Appendix I. Thermal Conductivity of Air at Reduced Pressures

The ratio of the thermal conductivity of air at reduced pressure to that at 1 bar can be approximated by [24]

$$\frac{K_{rp}}{K_0} = \left[1 + \frac{C}{P_p}\right]^{-1} \tag{I-1}$$

where C = 7.6 x 10^{-5} K m/N and the pressure parameter is given by $P_p = Pd/T$. Here, P is the pressure (N/m^2 = Pa), d is the scale length (m), and T is the temperature (K). A plot of this equation is given in Figure I.1 While this formula essentially describes Low Pressure Theory only (the so-called Slip Flow Theory) and should be replaced by the Free Molecule Theory when the pressure parameter falls below 10^{-4}, the formula gives remarkably good results for much lower values. [20]

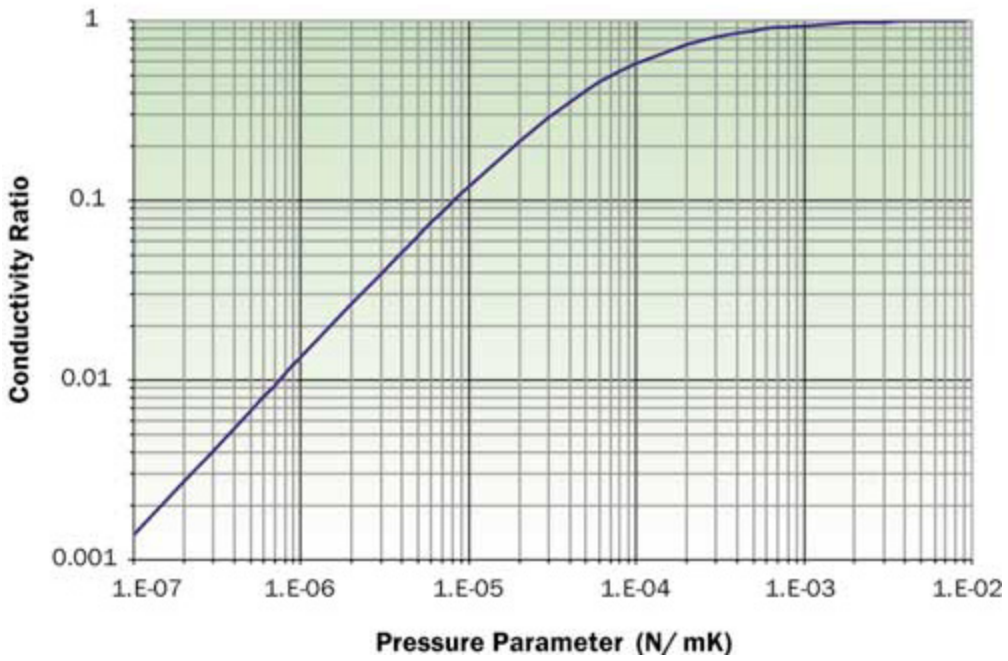

Figure I.1 Conductivity Ratio as a function of the pressure parameter from [20].

A well-maintained two-stage mechanical pump can reduce the pressure to 1 mT (= 0.1 Pa). However, the pump available to evacuate the jacket surrounding the test cell created a reduced pressure of only 5 Pa (40 mT). For a 1 cm scale length, this reduced the thermal conductivity of the air by only 30%, whereas a well-maintained two-stage rotary vane pump would have reduced by thermal conductivity of air factor of 24 from the atmospheric pressure value.

Appendix J. Technical Reports Addendum Asset Summary (TRAAS) Form (Equipment Calibration Information)

Technical Reports Addendum Asset Summary #2017091311405918365

Report Name: Nickel-Hydrogen Anomalous Heat Effect 2017091311405918365
JO: 8019-00
First Aerospace Author / PI: Edward J Beiting III

Created By: Edward J Beiting III

NON Aerospace MTE: All DC Voltage, DC Current, Temperature, and Pressure measurements were made with Rigol DAQ M300 Serial # = MM3A161550016 and Aerospace # = ADI269. Metrology was unable to calibrate this instrument and instructed me to perform a calibration using Metrology calibrated instrument. The following procedure was used.

DC Voltage Calibration
DC Voltage applied to M300 V = 0, 1, 2, 4, 8, 16, 32 V (max output of power supply used in experiment and in parallel with Agilent 34401A 6.5 digit Digital Multimeter ABE983 Calibration due date 2/21/2016. The M300 voltage and measured Agilent 34401A voltage values agreed to ± 0.002 V. .

DC Current Calibration
DC Current applied to M300 V = 0, 0.5, 1, 2, 4 V through 0.1 ohm resistor I = VM300/R (maximum of 4 A) in series with Agilent 34401A 6.5 digit Digital Multimeter ABE983 Calibration due date 2/21/2016. The currents agreed to ± 0.002 A.

Two identical type K thermocouples where placed in contact with each other and submerged in a liquied in a beaker place on a heating plate. The Rigol M300 temperature output values of the type K thermocouples were compared to an Omega HH309A thermocouple readout (Aerosppace # IBS ACH235, Cal Due Date 6/14/15) at 0o C (ice bath) and 241o C (hot glycerin). A linear correction was applied.

Pressure Transducers
A total of four pressure transducers were sent to the Aerospace Calibration Department for calibration. They sent them to PRIMARY STANDARDS NORTH AMERICA, INC. who provided calibration tables dated May 6, 2014. TD41 SN 1307 19027, Transducer Direct TD41 SN 1307 19028, Transducer Direct TD1000 SN 17822, Transducer Direct TD1000 SN 17824. Cal Due Date 3/1/15)

Technical Reports Addendum Asset Summary #2017091311405918365

ABE983 AGILENT 34401A MULTIMETER Usage Dates: 11/19/2014 - 02/19/2015

Calibration Date	Calibration Due Date	Certificate Number	Certificate Notes
06/27/2014	02/21/2016	895a4a84608edd42a9ef8b47ee679543	TMT-NORMAL

ACH235 OMEGA ENGINEERING COMPANY HH309A THERMOMETER Usage Dates: 11/19/2014 - 02/19/2015

Calibration Date	Calibration Due Date	Certificate Number	Certificate Notes
02/14/2014	06/14/2015	71189d1b595d774b8e67bc8b46fb3ee6	TMT-NORMAL

External Distribution

REPORT TITLE

Investigation of the Nickel-Hydrogen Anomalous Heat Effect

REPORT NO.	PUBLICATION DATE	SECURITY CLASSIFICATION
ATR-2017-01760	June 1, 2017	UNCLASSIFIED

Dr. Brian Ahern
Vibronic Energy
Technologies
ahern_brian@msn.com

Dr. Richard Garwin
IBM Research Laboratory
rig2@us.ibm.com

Dr. William Happer
Princeton University
happer@princeton.edu

Release to Public	Control Export
Yes ☑ No ☐	Yes ☐ No ☑

APPROVED BY_____ DATE_____
(AF OFFICE)

AEROSPACE REPORT NO.
ATR-2017-01760

Investigation of the Nickel-Hydrogen Anomalous Heat Effect

Cognizant Program Manager Approval:

James P. Nokes, PRINC DIRECTOR
SPACE MATERIALS LABORATORY
PHYSICAL SCIENCES LABORATORIES
ENGINEERING & TECHNOLOGY GROUP

Aerospace Corporate Officer Approval:

Charles L. Gustafson, SR VP ENG & TECH
ENGINEERING & TECHNOLOGY GROUP

Content Concurrence Provided Electronically by:

Edward J. Beiting, MTS RET CASUAL R3
ELECTRIC PROPULSION & PLASMA SCIENCE
PROPULSION SCIENCE DEPT
SPACE MATERIALS LABORATORY

Office of General Counsel Approval Granted Electronically by:

Domenic C. Rigoglioso, ASSOC GEN COUNSEL
OFFICE OF THE GENERAL COUNSEL
OFFICE OF GENERAL COUNSEL & SECRETARY

© The Aerospace Corporation, 2017.

All trademarks, service marks, and trade names are the property of their respective owners.

ST0218

AEROSPACE REPORT NO.
ATR-2017-01760

Investigation of the Nickel-Hydrogen Anomalous Heat Effect

Export Control Office Approval Granted Electronically by:

Edward Pevzner, EXPORT CONTROL STAFF IV
GOVERNMENT SECURITY
SECURITY OPERATIONS
OFFICE OF THE CHIEF VELOCITY OFFICER

© The Aerospace Corporation, 2017.

All trademarks, service marks, and trade names are the property of their respective owners.

ST0218